REDUCED-ORDER EXTENDED STATE OBSERVER AND FREQUENCY RESPONSE ANALYSIS

GANG TIAN

Bachelor of Science in Electrical Engineering

Beijing University of Posts and Telecommunications

July, 1997

submitted in partial fulfillment of the requirements for the degree

Master of Science in Electrical Engineering

at the

CLEVELAND STATE UNIVERSITY

May 2007

This thesis has been approved for the

Department of **ELECTRICAL AND COMPUTER ENGINEERING**

and the College of Graduate Studies by

_____

Thesis Committee Chairperson, Dr. Zhiqiang Gao

_____

Department/Date

_____

Dr. Wenbing Zhao

_____

Department/Date

_____

Dr. Lili Dong

_____

Department/Date

_____

Dr. F. Eugenio Villaseca

_____

Department/Date

To my loved wife Fei and new family...

ACKNOWLEDGMENTS

I would like to thank the following people:

Dr. **Zhiqiang Gao** for all his full-of-insight guidance as my supervisor, and for the virtues I learned from him.

Dr. **F. Eugenio Villaseca** and Dr. **Lili Dong** for their patience to convey the fundamental knowledge in the first semester.

Dr. **Wenbing Zhao**, Dr. **Pong P. Chu**, and Dr. **Dan Simon** for their elaborately prepared lectures which imparted knowledge to me, and their perspectives of different things that enriched my view.

Dr. **George L. Kramerich** for his jokes, for his encouraging me to practice oral English language, and for his effort to make me strong.

Dr. **Mary Murray** for my improvement in English writing and better understanding of American culture.

Qing Zheng, **Jeff Csank**, **Wankun Zhou**, **Aaron Radke**, and **Robert Miklosovic** for their kind help and friendship.

I would also thank my wife Fei. She supported me all the time.

REDUCED-ORDER EXTENDED STATE OBSERVER AND FREQUENCY RESPONSE ANALYSIS

GANG TIAN

ABSTRACT

This work provides a survey of different disturbance estimation and rejection methods, proposes a Reduced-order Extended State Observer (RESO), and carries out the frequency response analysis of Active Disturbance Rejection Control (ADRC). An extensive literature review of ADRC and other disturbance rejection methods is first given to provide the background of the research. Compared to the other disturbance rejection methods reviewed in this thesis, ADRC is the only method that can deal with nonlinear time-varying plants and can estimate and reject both external disturbances and unknown dynamics in the system. Relationship between ADRC and the other disturbance rejection methods are also established through the comprehensive study. Then a new controller, the ADRC with RESO, is proposed to decrease phase lag, which is common in observer-based controller design. The transfer functions under two-degree-of-freedom structure are also derived for this new controller for analysis. Finally, based on the transfer functions, frequency response of ADRC system is analyzed for a second-order linear time-invariant plant.

TABLE OF CONTENTS

Page

ABSTRACT v

LIST OF TABLES ix

LIST OF FIGURES x

NONMENCLATURE xii

ACRONYM xvii

CHAPTER

I. INTRODUCTION 1

II. LITERATURE REVIEW 6

2.1 Terminology 6

2.1.1 Plant Information or Dynamics 6

2.1.2 Disturbances 7

2.1.3 Feedforward and Feedback 9

2.2 Active Disturbance Rejection 11

2.3 Active Disturbance Rejection Control 12

2.3.1 Structure 13

2.3.2 Features 16

2.3.3 Implementations 17

2.4 Other Disturbance Rejection Methods 23

2.4.1 Internal Model Control 23

2.4.2 Unknown Input Observer 25

2.4.3 Disturbance Observer 28

2.4.4 Perturbation Observer 32

2.4.5 Model Estimator 34
2.5 Comparisons of active disturbance rejection methods 36
2.5.1 Disturbance rejection diagram 36
2.5.2 Equation equivalence 37
2.5.3 General comparison 39
III. REDUCED-ORDER EXTENDED STATE OBSERVER 41
3.1 Reduced-order Extended State Observer 42
3.2 Generalization of ADRC controller with RESO 45
3.3 Transfer Function Derivation 49
3.3.1 Procedure 51
3.3.2 Results 52
3.3.3 Analysis 53
IV. FREQUENCY RESPONSE ANALYSIS OF ADRC 56
4.1 ADRC with ESO 57
4.1.1 Bandwidth and Stability 58
4.1.2 Loop Gain Frequency Response 59
4.1.3 External Disturbance Rejection 62
4.2 ADRC with RESO 63
V. SUMMARY AND FUTURE RESEARCH 69
5.1 Conclusions 69
5.2 Future Research 71
BIBLIOGRAPHY 72
APPENDIX 76
A. TRANSFER FUNCTION DERIVATION 77
A.1 Relative order of ESO Equals to one 78
A.1.1 ESO estimation after disturbance cancellation 78

A.1.2 2-dof transfer function derivation 80
A.2 Relative Order of ESO is Greater Than One 82
A.2.1 ESO estimation after disturbance cancellation 82
A.2.2 2-dof transfer function derivation 89
A.3 Merge 92

LIST OF TABLES

Table		Page
I	PDESO and CDESO coefficient matrices	22
II	Comparison of ADRC, IMC, DoB, UIO, PoB, and ME	39
III	Mapping between DoB and parameterized ESO	53
IV	Gain Margin and Phase margin under different a_0 (3^{rd}-order ESO) .	59
V	Gain Margin and Phase margin under different a_1(3^{rd}-order ESO) . .	60

LIST OF FIGURES

Figure		Page
1	Conventional Closed-loop Control System Diagram	7
2	General Closed-loop Control System with Disturbance Diagram	8
3	Feedback and feedforward system diagram	10
4	The ADRC Structure	13
5	Comparison between linear and nonlinear gains (left: $\alpha = 1/3$ for k_P or K_I right: $\alpha = 3$ for k_D)	18
6	Comparison between linear, nonlinear, and fal gains($\alpha = 1/3$, $\delta = 0.3$)	19
7	IMC diagram(1-dof)	23
8	IMC diagram(2-dof)	24
9	UIO diagram	26
10	DoB disturbance rejection diagram	29
11	DoB diagram	31
12	Feedback Interpretation of the DoB	31
13	Diagram of general disturbance estimator	36
14	DoB in IMC form	37
15	ADRC with Single-loop ESO Block Diagram	45
16	Compensated plant Block Diagram	51
17	2-dof (U_0) Block Diagram	51
18	2-dof (U) Block Diagram	52
19	Stability of ADRC in a_0-a_1 plane (3^{rd}-order ESO)	59
20	Loop Gain Bode Plots for $a_0 = [0, 0.1, 1, 10, 100]$ (3^{rd}-order ESO)	60

21 Loop Gain Bode Plots for $a_1 = [0.1, 1, 3.085, 10, 100]$ (3^{rd}-order ESO) 61

22 Loop Gain Bode plots for different a_1 and a_0(3^{rd}-order ESO) 61

23 Bode plots of $G_{dy}(s)$ for $a_0 = [0, 0.1, 1, 10, 100]$ (3^{rd}-order ESO) . . . 62

24 Bode plots of $G_{dy}(s)$ for $a_1 = [0.1, 1, 3.085, 10, 100]$($3^{rd}$-order ESO) . 63

25 Stability of ADRC(2^{nd}-order RESO) in a_0-a_1 plane 64

26 Stability of ADRC(1^{st}-order RESO) in a_0-a_1 plane 65

27 Loop Gain Bode Plots for $a_0 = [0, 0.1, 1, 10, 100]$ (2^{nd}-order ESO) . . 65

28 Loop Gain Bode Plots for $a_1 = [0.1, 1, 3.085, 10, 100]$ (2^{nd}-order ESO) 66

29 Loop Gain Bode Plots for $a_0 = [0, 0.1, 1, 10, 100]$ (1^{st}-order ESO) . . 66

30 Loop Gain Bode Plots for $a_1 = [0.1, 1, 3.085, 10, 100]$ (1^{st}-order ESO) 67

31 Bode plots of $G_{dy}(s)$ for ADRC (3^{rd}-order, 2^{nd}-order, and 1^{st}-order ESO) 68

NOMENCLATURE

α_P, α_I, α_D Exponential parameters in Nonlinear gain function

β Discrete time domain pole location, equals to $e^{-\omega_o t}$

δ Bound in fal function within which the gain is linear

ϵ Original plant states in ME

η Plant states that are not observable in ME

Γ Input matrix of the plant discrete state space model

Γ^+ Pseudo inverse matrix operator of Γ

$\hat{b}$ Estimation of b

$\hat{d}$ Estimation of d

$\hat{f}$ Estimation of f

$\hat{G}_d(s)$ Nominal model of $G_d(s)$

$\hat{G}_p(s)$ Nominal plant transfer function, represent the nominal plant

$\mathbf{z}$ $\mathbf{z}$ transform variable

$\mathcal{G}$ Nonlinear gain vector of ADRC

$\mathcal{L}$ Laplace transform operation

ω_o Observer bandwidth

Φ System matrix of the plant discrete state space model

Ψ	Polynomial used in ADRC transfer function derivation
ρ	Ratio between b and $\hat{b}$
ξ	intercourse state in ME
A	System matrix of the plant state space model
A_d	System matrix for disturbance differential equation in UIO
a_i	Coefficients in plant differential equations. $i = 0 : n-1$
A_x	System matrix of the augmented plant state space model
A_z	System matrix of the ESO state space model
B	Input matrix of the plant state space model
b	Scaling factor from u to $y^{(n)}$ in n^{th}-order linear plant
b_i	Coefficients in plant differential equations. $i = 0 : n-1$
B_x	Input matrix of the augmented plant state space model
B_z	Input matrix of the ESO state space model
C	Output matrix of the plant state space model
C_d	Output matrix for disturbance differential equation in UIO
C_x	Output matrix of the augmented plant state space model
C_z	Output matrix of the ESO state space model
d	External disturbance
E	Matrix of the augmented plant state space model to introduce $f^{(n)}$.

e error signal

e_P, e_I, e_D Proportional error, Integral error, and derivative error

f Generalized Disturbance

$F(s)$ Internal dynamics to be rejected

$fal(x, \alpha, \delta)$ Nonlinear function applied in ADRC

$G_c(s)$ Feedback controller

$G_d(s)$ External disturbance pre-filter

$G_n(s)$ Equivalent noise pre-filter in 2-dof structure

$G_p(s)$ Plant transfer function, represent the real plant

$G_{c0}(s)$ Controller in 2-dof control structure with respect to u_0

$G_{c1}(s)$ The equivalent 2-dof controller of ADRC with 1^{st}-order ESO

$G_{c2}(s)$ The equivalent 2-dof controller of ADRC with 2^{nd}-order ESO

$G_{c3}(s)$ The equivalent 2-dof controller of ADRC with 3^{rd}-order ESO

$G_{dy}(s)$ Transfer function from d to y

$G_{lg}(s)$ Open-loop Transfer function from u to y

$G_{ny}(s)$ Transfer function from n to y

$G_{p0}(s)$ Transfer function from u_0 to y

$G_{ry}(s)$ Closed-loop Transfer function from r to y

$G_{u_0y}(s)$ Transfer function from u_0 to y

h Number of extended states in ESO

$H(s)$ Set-point pre-filter in 2-dof control structure with respect to u

$H_0(s)$ Set-point pre-filter in 2-dof control structure with respect to u_0

$H_1(s)$ The equivalent 2-dof set-point filter of ADRC with 1^{st}-order ESO

$H_2(s)$ The equivalent 2-dof set-point filter of ADRC with 2^{nd}-order ESO

$H_3(s)$ The equivalent 2-dof set-point filter of ADRC with 3^{rd}-order ESO

I Identity matrix

k_D Derivative Gain of PID

k_I Integral Gain of PID

k_P Proportional Gain of PID

L Observer gain matrix

L_c Error compensation gain matrix for Current Estimator

L_p Observer gain matrix for Predictive Estimator

m Order of ESO

n Measurement noise

n Relative order of the plant (when used in superscript or subscript)

$Q(s)$ Low pass filter, abbreviated as Q

$q(s)$ Controller in IMC

$q_d(s)$ Filter designed for disturbance rejection in 2-dof IMC

q_i Coefficients in disturbance differential equation in UIO, $i = 0 : h - 1$

$q_r(s)$ Set-point filter in 2-dof IMC, equals to $q(s)$

r Reference signal or set-point

s Laplace variable

$sign(x)$ Switch function

T Sampling time in discrete system

u Control signal

V Matrix of ESO state space model to obtain the $\hat{f}$

w the row number of the vector or the matrix

x state vector of the plant state space model

y Output vector of the state space model, in this thesis, the output

z state vector of the observer state space model

ACRONYM

ADRC Active Disturbance Rejection Control

CDESO Current Discrete Extended State Observer

CE Current Estimator

DAC Disturbance Accommodation Control

DEF Disturbance Estimating Filter

DoB Disturbance Observer

1-dof one-degree-of-freedom

ESO Extended State Observer

FBPO Feedback Perturbation Observer

FFPO Feedforward Perturbation Observer

IMC Internal Model Control

LHP Left Half Plane

LTI linear time-invariant

ME Model Estimator

MIMO Multiple-Input and Multiple-Output

MPEC Multiloop Perturbation Compensation

NTV nonlinear time-varying

PD Proportional-Derivative

PDESO Predictive Discrete Extended State Observer

PE Predictive Estimator

PID Proportional-Integral-Derivative

PoB Perturbation Observer

RESO Reduced-order Extended State Observer

SISO Single-Input and Single-Output

SMPO Sliding Mode Perturbation Observer

TDE Time-Delayed Estimator

UIO Unknown Input Observer

CHAPTER I

INTRODUCTION

With the birth of *Cybernetics* [1] in 1948, pioneered by Norbert Wiener, *feedback* control theory was established and was accepted by most researchers. From then on, led by different concerns of engineers and mathematicians, various branches of control methods were developed and continue to be developed.

Categorized by the information required to design controllers, control methods can be put into two classes: *model-independent* methods, such as Proportional-Integral-Derivative (PID), and *model-based* control methods, such as loop shaping, pole placement and other modern control methods.

Simple and effective, without need of plant information, the PID controller is dominant in industry [2]. This control technique enables technicians to tune the three parameters (k_P, k_I, and k_D) for different systems easily and rapidly without math knowledge of plant dynamics. However, the ever increasing demands for accuracy, robustness, and efficiency, coupled with the inherent limitations of PID, have driven engineers to seek better control mechanisms elsewhere.

On the other hand, modern control methods, dominant in academy, need ac-

curate plant information, such as loop-shaping and optimal control. Given a nominal plant model, these *model-based* control methods can produce "perfect" controllers to control the plant as the designer desired. These "perfect" controllers, however, are perfect only for the case where the real plant matches the nominal plant. When the plant dynamics change, the "perfect" performance is gone. The question is, how much changes in plant dynamics can these *model-based* methods handle. Another drawback of *model-based* control methods is the specific design, which needs to be carried out every time when the controller is implemented in a new plant. Thus, technicians in the industry need to have enough knowledge of advanced mathematical developments to design and tune these *model-based* controllers. These two reasons restrain modern control methods from being widely applied in industry.

Actually, humankind's knowledge of the real world is somewhere between zero and infinity. The reality of human beings' knowledge leads researchers to a new class of control methods, denoted as *partial-model-based* methods. In this new class, controller design relies only on the known part of the plant information, while the unknown part of the plant information is treated as uncertainties.

Within the *partial-model-based* method class, there are also two different ways to deal with the unknown part of the plant information. The disturbance can be rejected passively, such as robust control, adaptive control, and intelligent control. For example, in robust control, controllers are designed based on the expected uncertainty or modeling errors. The successfulness of this control method relies on the ability of the designer to accurately describe the amount of the uncertainties in the plant[3].

Disturbance can also be rejected actively. In another words, external disturbances and uncertainties are estimated and compensated for in real time. Such active disturbance rejection methods present strong robustness against the discrepancy between the limited plant information and the real plant, which is not discussed in

the *model-based* methods. Active Disturbance Rejection Control (ADRC) belongs to this class. It is a relatively new, and quite different design concept that shows much promise in obtaining consistent response in a nonlinear time-varying (NTV) industrial control system full of uncertainties, where both the external disturbances and the unknown dynamics are estimated and rejected. The stability of ADRC in plants with uncertainties are proved, which establishes a solid base for ADRC applications. But most of the development and analysis has only been shown in the time-domain due to its original nonlinear gain design. A lack of comprehensive understanding of ADRC's frequency response characteristics makes it difficult to compare ADRC and other disturbance rejection methods. Furthermore, as an observer-based method, the Extended State Observer (ESO) in ADRC introduces more phase lag when the observer order gets higher.

Another active disturbance rejection method is Model Estimator (ME), which is designed in state space to estimate the unknown dynamics. Although the stability proof of ME is provided with a specific plant model, the design of disturbance rejection in ME does not require nominal model.

There are also some other active disturbance rejection methods, which are *model-based* active disturbance rejection methods. Among these *model-based* active disturbance rejection methods are Internal Model Control (IMC), Disturbance Observer (DoB), Unknown Input Observer (UIO), and Perturbation Observer (PoB). Claims were made in some of these methods, such as DoB, that the discrepancy between the real plant and its nominal model can be compensated in the low frequency. But these methods were actually designed to estimate and reject external disturbances, and there is no proof for unknown dynamics rejection in these methods. Another drawback of these *model-based* active disturbance rejection methods is, because being designed for a certain nominal model, these methods are applied only

in linear time-invariant (LTI) systems.

ADRC, ME, and these *model-based* active disturbance rejection methods come from different control designs(*partial-model-based* or *model-based*, *feedback* or *feed-forward*, in time domain or in frequency domain, continuous-time or discrete-time). Due to the complexities and difficulties, only a few works were done in the past to relate these disturbance rejection methods and to make comparisons. Thus, despite the fact that there are many methods to reject disturbance, the research results of each method cannot benefit another.

To enrich existing ADRC methods, establish relationships among ADRC and the other active disturbance rejection methods, and allow frequency response analysis of ADRC, this research centers on the following three aspects:

First, compare ADRC to the other disturbance rejection methods. The equivalence and the difference between ADRC and the other disturbance rejection methods are distinguished.

Second, propose a new ADRC controller, the ADRC with Reduced-order Extended State Observer (RESO), to decrease phase lag in the observer. The active disturbance rejection methods normally employ a filter or an observer, which introduce phase lag into the system. Currently, the ESO in ADRC controllers is applied with full order. With the proposed ADRC controller, the ESO order can be reduced to decrease phase lag. Then the ADRC with RESO is extended to m^{th}-order with h extended states and dealing with n^{th}-order plant, the 2-dof transfer functions of which are also derived to facilitate the frequency response analysis.

Third, analyze the frequency response for ADRC. Based on the derived 2-dof transfer functions of the ADRC with RESO controller, frequency-domain analysis of ADRC is performed to quantify its performance and stability characteristics.

The organization of this thesis is as follows. First, the literature review is given

in *Chapter 2* to provide a comprehensive overview of different disturbance rejection methods and then to make comparisons among them. According to the idea behind the regular ADRC controller, in *Chapter 3*, RESO is proposed and its transfer functions is derived in a 2-dof structure. Finally, as an example, a frequency response analysis is carried out for ADRC controllers in *Chapter 4*.

CHAPTER II

LITERATURE REVIEW

In this chapter, first the definitions related to disturbance rejection are clarified. Then the origin and the development of different active disturbance rejection methods are reviewed. Finally comparisons are made among these methods.

2.1 Terminology

2.1.1 Plant Information or Dynamics

In control systems, plant information is the knowledge of the physical plant that people can obtain from input-output analysis or mathematical modeling of a physical plant. In mechanics, the plant information is also called dynamics, which are the forces and motions that can represent the characteristics of a system. Normally there are two ways to obtain information from a physical plant. One is to apply specific inputs, such as sinusoidal waves of different frequency, to the plant and measure the corresponding plant outputs, upon which the data are analyzed to construct a model. The other one is to derive mathematic models with scientific laws. The information

obtained is usually called a nominal model, which represents the knowledge of the plant that people can achieve. Actually, with the Bode plot, differential equations, and other tools, a good nominal model can often be obtained for a given plant.

No matter how much people know, however, there will still be something unknown; similarly, no matter how good the nominal model is, it is not the real plant. The unknown information, or the unknown dynamics, is not covered by the nominal model and thus causes uncertainties in the system. Thus, there are two parts in the dynamics of the system: the known dynamics, usually described in the nominal model, and the unknown dynamics, which is not accessible through plant analysis and system identification.

2.1.2 Disturbances

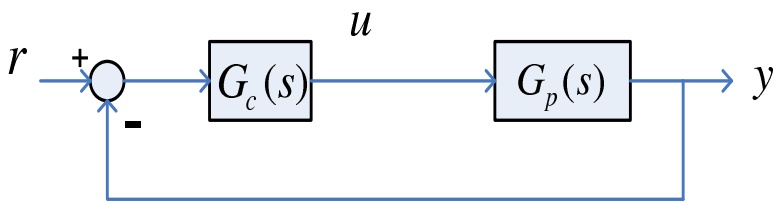

Figure 1: Conventional Closed-loop Control System Diagram

The block diagram of an ideal conventional closed-loop control system is shown in Figure 1 . Assume the plant is LTI and has an accurate mathematical model, denoted as $G_p(s)$, and there is neither external disturbance nor measurement noise. Such plant can be perfectly controlled by an appropriately designed controller $G_c(s)$. However, ideal case does not exist in the real world. Due to the limited knowledge of plant information and perturbation imposed by the environment, the nominal model differs from the real plant, which causes control difficulties, as shown in Figure 2.

As shown in the diagram in Figure 2, in the real world, four things make the ideal case described in Figure 1 impossible: the nonlinear time-varying (NTV) feature

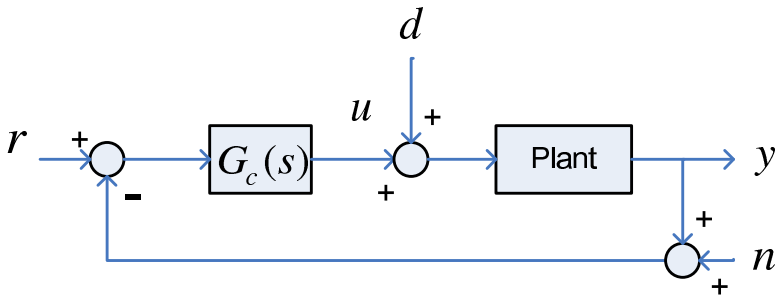

Figure 2: General Closed-loop Control System with Disturbance Diagram

of the real plant, the unknown system dynamics, the external disturbance d, and the measurement noise n , which are discussed respectively as follows.

Real plants are normally nonlinear and time-varying, which cannot be expressed by the transfer function $G_c(s)$ as in Figure 1. Designed for LTI systems which can be characterized in the frequency domain by transfer functions, the conventional controllers cannot deal with NTV plants.

The *external disturbance* is independent of system states. It includes the input disturbance and the output disturbance. The input disturbance is usually introduced into the control signal u. In the case where an external disturbance is added to the output of the plant and contribute to the system output y, it can be converted to the input disturbance. Such disturbances are external, not related to the system dynamics. All the active disturbance rejection methods discussed later in this chapter estimate and reject the *external disturbances* except for ME.

Not like the *external disturbances*, the *unknown dynamics* is related to the system states. The nominal model represents the known information of the plant. The discrepancies between the real plant and its nominal model are the unknown dynamics of the system. Compared to the other active disturbance rejection methods reviewed in this thesis, only ADRC and ME deal with *unknown dynamics*, as will be discussed later in this chapter.

Measurement noise is different from the above two perturbation source. Mea-

surement noise exists in closed-loop system. The system output is not directly available, therefore a sensor is required to measure the system output. During the measurement process, noise is introduced into the system through the feedback loop. Measurement noise is the signal of high frequency, which is normally rejected by limiting the bandwidth and maintaining low gain in high frequency in the loop gain of the system. Therefore, in this research, noise is separated from disturbance.

ADRC extended disturbance definition from the conventional *external disturbance* to the *generalized disturbance*, which includes the *external disturbance* and the *unknown dynamics*. Some of the other disturbance rejection methods may claim the compensation ability of the slight discrepancy between the real plant and its nominal plant. however, there is no conclusion on how much discrepancy can be tolerated in the system. The slight deviation from the nominal model in the other methods is also different from the *unknown dynamics* which is actively estimated and rejected in ADRC.

2.1.3 Feedforward and Feedback

Feedback

Although *feedback* control was used about thousands of years ago, its concept was established by Norbert Wiener[1]. *Feedback* can be negative or positive, depending on whether it has the same direction as the system output. With the same direction as the system output, positive *feedback* drives the system output farther away from the reference and is usually used to amplify signals. The negative *feedback*, on the contrary, is opposite to the system output. As a result, negative *feedback* forces the system output closer to the reference, which makes negative *feedback* to be the basis for tracking systems.

A typical negative *feedback* system is already shown in Figure 2. The system

output y is fed back to the *feedback* controller to force y to track r. *Feedback* control goes into effect after the appearance of an error. In another words, *feedback* control is a reactive control method.

Feedback control has a natural ability to reject *external disturbances*. The output y contains the information of the *external disturbance* d. Thus *external disturbance* can be rejected with an appropriately designed *feedback* controller. When d is rejected, however, the measurement noise n is introduced into the system through the *feedback* loop. Noise may cause worse performance and therefore is a concern in the *feedback* control design.

Feedforward

Like *feedback*, *feedforward* is also widely used in industry, especially in process control after 1960s. There are two types of *feedforward*: *set-point feedforward* and *disturbance feedforward*. The *feedback* and the two different types of *feedforward* are shown together in the following figure.

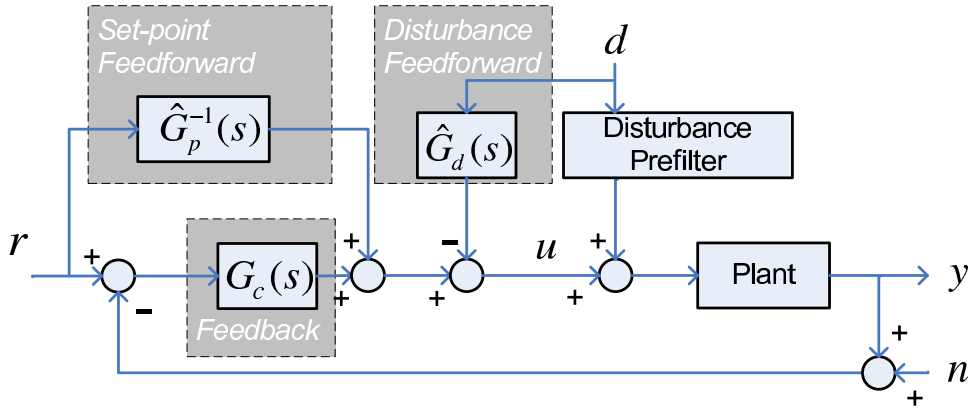

Figure 3: Feedback and feedforward system diagram

In process control, *feedforward* control rejects incoming *external disturbance* according to the nominal plant and disturbance models[4]. This kind of *feedforward* is *disturbance feedforward*. As shown in Figure 3, if the *external disturbance* d is

measurable and its model (the disturbance pre-filter) is known, denoted as $\hat{G}_d(s)$, the *external disturbance* can be compensated by the *disturbance feedforward* $\hat{G}_d(s)$ in the system. However, the assumption that d is measurable is hard to satisfy in reality. Thus modified disturbance compensation methods are developed, such as the *fictitious disturbance generator* in UIO and the $q_d(s)$ design in IMC which will be discussed later in this chapter.

Figure 3 also shows the other type of *feedforward*: the *set-point feedforward*. Assume there is no disturbance and the nominal model $\hat{G}_p(s)$ matches the real plant model perfectly, *feedback* is no longer needed if the inverse of the plant is applied to get the transfer function equal to one from the reference signal r to output y. This technique is used widely in industry, such as the velocity feedforward and the acceleration feedforward in motion control system. Since the nominal model cannot be the same as the real plant, the *set-point feedfoward* is used together with the *feedback* in industrial tracking systems.

Not like *feedback* control, *feedforward* control is a proactive method that operates before error occurs according to the nominal model.

2.2 Active Disturbance Rejection

Since disturbances are unwanted in control systems, they need to be rejected. A common feature in different disturbance rejection methods is that the *external disturbances* are estimated in a certain way and are compensated in the control signal. To estimate the disturbances, more or less plant information is needed. The needed plant information is quite different for the *model-based* active disturbance rejection methods and ADRC.

Originating from *model-based* methods, the *model-based* active disturbance rejection methods are LTI and estimate *external disturbances* based on the precise

nominal model. Such methods include IMC, DoB, UIO, PoB.

ADRC is quite different from these disturbance rejection methods which are designed for LTI systems and need a precise nominal model. ADRC is designed in time-domain and can deal with NTV plants. Only the minimum plant information is needed in ADRC. The *unknown dynamics* in ADRC is not the small deviation from the nominal model in these *model-based* disturbance rejection methods. Indeed, the *unknown dynamics* in ADRC includes the part of system dynamics that need to be rejected to get the system behave as cascaded integrators.

Theoretically, the more precise the nominal model is, the better its performance is. However, most physical plants are time-varying, which cannot be described by the LTI nominal models that are used in these *model-based* disturbance rejection methods. In this sense, more information introduced in the linear nominal models does not help the control performance.

Furthermore, even if the physical plants are not time-varying, the required modeling work prevents the *model-based* active disturbance rejection methods from wide applications. For example, a servo motor may drive different kinds of loads, which greatly change the dynamics of the system. In this case, *model-based* active rejection methods need to be redesigned for each case.

The details of each active disturbance rejection method studied in this research are reviewed in the following sections.

2.3 Active Disturbance Rejection Control

ADRC was first proposed by J. Han in 1990s [6]-[10]. The active disturbance rejection concept was first introduced in the English literature in [11] and further simplified and explained in [12] and [13], respectively. The central idea is that both the internal dynamics and *external disturbances* can be estimated and compensated for in

real time. This estimation is a drastic departure from the existing *model-based* design paradigm since the information of the physical process needed by the controller is obtained from the plant input-output data, not from an a priori mathematical model. This new design framework applies generally to NTV systems with Single-Input and Single-Output (SISO) or Multiple-Input and Multiple-Output (MIMO).

ADRC was originally formulated using nonlinear gains (reviewed in the subsection 2.3.3), which makes the frequency response analysis difficult. The simplification of ADRC in [12] using linear and parameterized gains provides a much needed, easy-to-implement formulation. More importantly, it enables a thorough evaluation of ADRC in the frequency domain.

Discrete version of parameterized ADRC was proposed by R. Miklosovic *et al* in 2006[14]. W. Wang *et al* compared a nonlinear ADRC with DoB in a hydrolic position servo system in 2004 to show the advantage of ADRC over DoB[15]. A. Radke produced a survey on different observers and proposed KESO in 2006, which is an optimized ESO implementation [16]. The stability proof of ADRC was conducted by Q. Zheng *et al* in 2007[17]. Q. Zheng *et al* also proposed a dynamic decoupling control approach based on ADRC for MIMO systems[18].

2.3.1 Structure

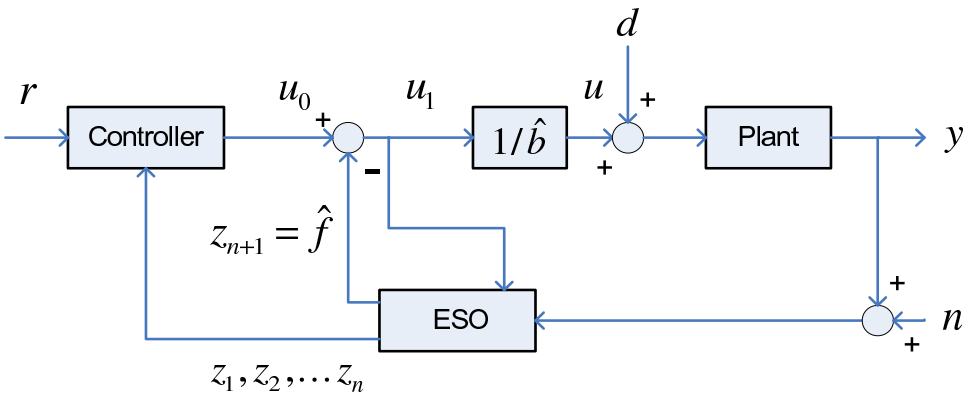

Figure 4: The ADRC Structure

In ADRC, the required plant information is the relative order of the plant and the system gain, which is a simplification from an accurate mathematical model that is required by *model-based* methods. ADRC forces the plant to behave as a desired simple plant, a series of cascaded integrators. The internal dynamics are treated as an internal disturbance. This internal disturbance is included with the *external disturbances* to form the *generalized disturbance*. The goal of ADRC is to estimate and reject the *generalized disturbance*.

The idea of ADRC is illustrated by a typical parameterized ADRC control algorithm implementing on second-order system, which is generalized by Z. Gao in [12] and [13]. Consider a general second-order plant:

$$\ddot{y} = f\left(y, \dot{y}, d, t\right) + bu \tag{2.1}$$

where y is system output, u is control signal, b is a constant, d is input disturbance.

Under the ADRC framework, the entire $f\left(y, \dot{y}, d, t\right)$ can be looked on as a *generalized disturbance*. If this *generalized disturbance* can be cancelled, the system is reduced to a simple double-integral plant with a scaling factor b, which can be easily controlled.

In ADRC , the required estimate of the plant gain b, known as $\hat{b}$, is roughly known. Therefore, the scaling factor b can be removed by introducing the inverse of its estimation in the control law: $u = \frac{1}{\hat{b}} u_1$, as shown in Figure 4. Now (2.1) changes to the following equation.

$$\ddot{y} = f\left(y, \dot{y}, d, t\right) + u_1 \tag{2.2}$$

To capture the information of $f\left(y, \dot{y}, d, t\right)$ and cancel it from the system dynamics leads to the Extended State Observer (ESO).

The model of (2.2) can be written in state space form and extended to include an additional state $f(y, \dot{y}, d, t)$, simply presented by f. Let $x_1 = y$, $x_2 = \dot{y}$, and

$x_3 = f$, the extended plant state space model can be written as follows.

$$\begin{cases} \dot{x} = A_x x + B_x u_1 + E\dot{f} \\ y = C_x x \end{cases} \tag{2.3}$$

where:

$$A_x = \begin{bmatrix} 0 & 1 & 0 \\ 0 & 0 & 1 \\ 0 & 0 & 0 \end{bmatrix}, B_x = \begin{bmatrix} 0 \\ 1 \\ 0 \end{bmatrix}, E = \begin{bmatrix} 0 \\ 0 \\ 1 \end{bmatrix}, C_x = \begin{bmatrix} 1 & 0 & 0 \end{bmatrix}$$

In the extended state space model of the plant (2.3), the only unknown part is $\dot{f}$. In observer designs, this unknown part is normally omitted and automatically compensated by the observer error correction. With z_1, z_2, and z_3 tracking x_1, x_2, and x_3 respectively, The ESO is employed to estimate f:

$$\begin{cases} \dot{z} = A_z z + B_z u_1 + L\left(y - C_z z\right) \\ \hat{f} = Vz \end{cases} \tag{2.4}$$

where $A_z = A_x$, $B_z = B_x$, $C_z = C_x$, $V = [0\ \ 0\ \ 1]$, and the observer gains, which are obtained by solving the equation $\lambda(s) = |sI - A_x + LC_x| = (s + \omega_o)^3$, are chosen to get all the eigenvalues equal to the observer bandwidth ω_o, and located in the Left Half Plane (LHP), which yields only one parameter for ESO tuning [12]:

$$L = \begin{bmatrix} l_1 & l_2 & l_3 \end{bmatrix}^T, l_1 = 3\omega_o, l_2 = 3\omega_o^2, l_3 = \omega_o^3 \tag{2.5}$$

With a well-tuned observer, z_1, z_2 and z_3 will track y, $\dot{y}$ and f respectively: $z_1 \approx y$, $z_2 \approx \dot{y}$ and $z_3 \approx f$. The *general disturbance* f is rejected by applying $u_1 = u_0 - z_3$. A linear Proportional-Differential(PD) control law $k_P e + k_D \dot{e}$ is then applied together with *the set-point feedforward* $\ddot{r}$ to control the pure double-integral plant:

$$u_0 = k_P\left(r - z_1\right) + k_D\left(\dot{r} - z_2\right) + \ddot{r} \tag{2.6}$$

The control law (2.6) is designed to achieve an unity gain closed-loop system, which is straightforward by substituting $z_1 \approx y$ and $z_2 \approx \dot{y}$ into (2.6) and then substituting (2.6) into (2.1):

$$\ddot{y} + k_D\dot{y} + k_P y = \ddot{r} + k_D\dot{r} + k_P r \tag{2.7}$$

which will yields $y = r$.

For simplicity, the controller gains k_P and k_d are parameterized with one tuning parameter ω_c for critically damped response: $k_P = \omega_c^2, k_D = 2\omega_c$[12].

2.3.2 Features

The essence of ADRC is to force the plant to behave as a series of cascaded integrators and then control it. Fundamental difference between ADRC and these *model-based* active disturbance rejection methods is: these *model-based* active disturbance rejection methods try to force the plant to behave as the nominal plant, while ADRC reduces the plant to a simple plant, a series of cascaded integrators, by estimating and rejecting *general disturbance* f. The simple plant reduced by ADRC brings simple tuning. In the parameterized ADRC, there are only two parameters to be tuned. One is the observer bandwidth, ω_o, and the other one is the control bandwidth, ω_c.

Another advantage of ADRC is the ability to deal with NTV plants. In ADRC, the difference between the real plant and the cascaded integrators, no matter linear or nonlinear, time-invariant or time-varying, are estimated by the ESO. The ESO is not constrained by the limitation of linear designs in other active disturbance rejection methods, such as IMC, DOB, UIO, PoB, and ME.

In ADRC, the ESO estimates not only the *generalized disturbance*, but also the states. The states are fed back to the controller rather than feeding back the output. Thus, ADRC is a state feedback control algorithm. However, ADRC can

become a output feedback controller if only the estimated *generalized disturbance* is used in control law.

A significant advantage of ADRC is its proved stability. In [17], it is proved that, for an n^{th}-order plant, the estimation error of ESO 1) converges to the origin asymptotically when the model of the plant is available ; 2) is bounded and inversely proportional to the bandwidth of the observer when the plant model is mostly unknown.

2.3.3 Implementations

Nonlinear PID and Observer Gains

In PID control, the error between the reference and the output, the derivative of the error, and the integration of the error, are weighted to generate a control signal to force the output to track the reference. In the classical PID and the other linear control algorithms, the weights or gains, are constants which are simple and easy to implement.

However, linear gains limit the performance of the system in two aspects. First, the integral of the error are expected to be effective when the error is very small. When the error is very large, the integral of the error may cause the control signal saturation problem. Constant proportional gain also faces the saturation problem when the error is large. Second, the derivative of the error needs to be active when the error is large in order to prevent overshoot. But when the error is small, normally in steady state, the derivative of the error only contributes noise and should be ineffective. Therefore, the PID gains must be limited to avoid the problem just discussed.

To improve the performance, Han created a nonlinear mechanism in [6], to replace the linear gains in the controller, as shown in (2.8).

$$u = k_P|e_P|^{\alpha_P} sign(e_P) + K_I|e_I|^{\alpha_I} sign(e_I) + k_D|e_D|^{\alpha_D} sign(e_D) \tag{2.8}$$

where e_I and e_D are the integral and the derivative of the error e_P respectively.

To avoid the problems in classical PID control, the parameters are chosen as follows: $0 < \alpha_I < 1$, $0 < \alpha_P < 1$, and $\alpha_D > 1$. Therefore, when the error and its integral are large, the proportional correction item in (2.8), $k_P|e_P|^{\alpha_P} sign(e_P)$, and the integral correction item (2.8), $K_I|e_I|^{\alpha_I} sign(e_I)$, are bounded instead of increasing proportionally with the error and its integral respectively; the derivative correction item in (2.8), $k_D|e_D|^{\alpha_D} sign(e_D)$, approaches zero when the derivative of the error is small, as shown in Figure 5.

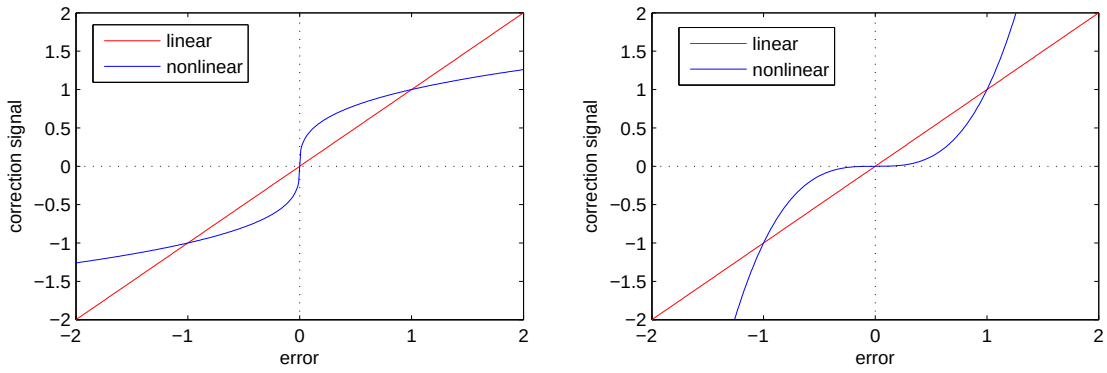

Figure 5: Comparison between linear and nonlinear gains (left: $\alpha = 1/3$ for k_P or K_I right: $\alpha = 3$ for k_D)

Along with the benefits obtained from the nonlinear gains shown in Figure 5, an infinity gain problem exists for the proportional correction item and the integral correction item when the error and its integral are near zero. To address this problem, Han proposed the $fal(x, \alpha, \delta)$ function, in which the gain is linear when the error falls into a small region around zero with bound δ, as shown in Figure 6.

The form of the fal function is shown as follows.

$$fal(x, \alpha, \delta) = \begin{cases} |x|^{\alpha} sign(x), |x| > \delta \\ x/\delta^{1-\alpha}, |x| \leq \delta \end{cases} \tag{2.9}$$

where $\delta > 0$. With the fal function to replace the linear k_P and k_D in (2.6), a

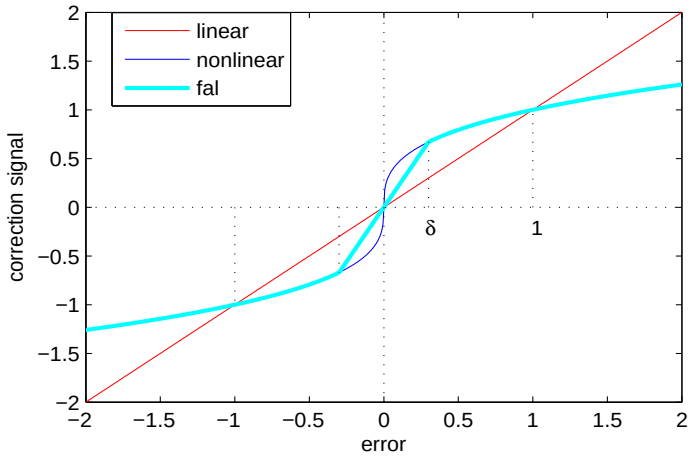

Figure 6: Comparison between linear, nonlinear, and fal gains($\alpha = 1/3$, $\delta = 0.3$)

nonlinear Proportional-Derivative (PD) controller is applied:

$$u_1 = k_P fal(r - z_1, \alpha_P, \delta_P) + k_D fal(\dot{r} - z_2, \alpha_D, \delta_D) + \ddot{r} - z_3 \tag{2.10}$$

Also, fal is applied to substitute the linear observer gains in (2.5). Thus, an nonlinear-gain ESO is generated, as shown in the following equation.

$$\begin{cases} \dot{z} = A_z z + B_z u_1 + \mathcal{G} \\ \hat{f} = Vz \end{cases} \tag{2.11}$$

where

$$\mathcal{G} = \begin{bmatrix} l_1 fal\left(z_1 - y, \alpha_1, \delta\right) \\ l_2 fal\left(z_1 - y, \alpha_2, \delta\right) \\ l_3 fal\left(z_1 - y, \alpha_3, \delta\right) \end{bmatrix}$$

Actually, the combination of (2.10) and (2.11), that is, ADRC with nonlinear gains, is the original form of ADRC.

Multiple Extended States

In the original ADRC, there is only one extended state in ESO. R. Miklosovic *et al* proposed an ESO with multiple extended states to improve the disturbance

rejection ability of ADRC when the disturbance type is not the step, for example, a ramp or a sinusoid[14].

The example plant in (2.1) is used again to illustrate the multiple-extended-state ESO. Assume the external disturbance is a ramp signal. To estimate the external disturbance along with the unknown dynamics, one more extended state, $x_4 = \dot{f}$, is introduced to augment the state space model in (2.3). The new extended state space model is written as follows:

$$\begin{cases} \dot{x} = A_x x + B_x u_1 + E\ddot{f} \\ y = C_x x \end{cases} \tag{2.12}$$

where:

$$A_x = \begin{bmatrix} 0 & 1 & 0 & 0 \\ 0 & 0 & 1 & 0 \\ 0 & 0 & 0 & 1 \\ 0 & 0 & 0 & 0 \end{bmatrix}, B_x = \begin{bmatrix} 0 \\ 1 \\ 0 \\ 0 \end{bmatrix}, E = \begin{bmatrix} 0 \\ 0 \\ 0 \\ 1 \end{bmatrix}$$

and $C_x = \begin{bmatrix} 1 & 0 & 0 & 0 \end{bmatrix}$.

With z_1, z_2, z_3, and z_4 tracking x_1, x_2, x_3, and x_4 respectively, the 4^{th}-order ESO is employed to estimate f:

$$\begin{cases} \dot{z} = A_z z + B_z u_1 + L\left(y - C_z z\right) \\ \hat{\hat{f}} = Vz \end{cases} \tag{2.13}$$

where $A_z = A_x$, $B_z = B_x$, $C_z = C_x$ and $V = [0\ 0\ 1\ 0]$.

The same observer gain design technique in (2.12) is applied here to get the eigenvalues equal to the observer bandwidth w_o, located in the LHP:

$$L = \begin{bmatrix} l_1 & l_2 & l_3 & l_4 \end{bmatrix}^T, l_1 = 4\omega_o, l_2 = 6\omega_o^2, l_3 = 4\omega_o^3, l_4 = \omega_o^4 \tag{2.14}$$

The control law design is exactly the same as the one in *Section* 2.3.1. With the introduction of one more extended state in (2.12), the unknown part that needs to be compensated by the observer error correction changes from $\dot{f}$ to $\ddot{f}$.

Simulations show that the ADRC with two extended states in the ESO can estimate and reject a triangular disturbance (which represents bounded ramp signal) better than the ADRC with one extended state in ESO [14].

Discrete version

Almost all the modern control algorithms are implemented in digital computers or microprocessors. To be implemented in a digital environment, control algorithms designed in the continuous-time domain need to be digitized first. A common way of digitization is to approximate the differential equations to difference equations by treating the sample value change rate of a signal over one sampling period as its derivative. For example, assuming $\dot{f} \approx 0$, the plant state space model in (2.3) can be approximated to the discrete version as shown in the following equation.

$$\begin{cases} x(k+1) = \Phi x(k) + \Gamma u(k) \\ y(k) = Cx(k) \end{cases} \tag{2.15}$$

where:

$$\Phi = \begin{bmatrix} 1 & T & 0 \\ 0 & 1 & T \\ 0 & 0 & 1 \end{bmatrix}, \Gamma = \begin{bmatrix} 0 \\ bT \\ 0 \end{bmatrix}, C = \begin{bmatrix} 1 & 0 & 0 \end{bmatrix}$$

The ESO form in (2.4) can also be approximated to the discrete version as shown in the following equation.

$$\begin{cases} z(k+1) = \Phi z(k) + \Gamma u(k) + L_p \left(y(k) - z_1(k) \right) \\ \hat{y}(k) = Cz(k) \end{cases} \tag{2.16}$$

where

$$L_p = \begin{bmatrix} 3\omega_o T & 3\omega_o^2 T & \omega_o^3 T \end{bmatrix}^T, \tag{2.17}$$

Here the design skill that put all the poles at ω_o is still applied in continuous time domain. Actually, pole location can be determined in **z** domain directly in

discrete design[19]. Besides the so-called Predictive Estimator (PE), the design of which is the same as the ESO described in (2.16), G.F. Franklin also discusses the Current Estimator (CE) in [19] . The ESO state space form of CE is the same as PE except for its output. In CE, part of the current estimator error is included in the estimator outputs to decrease the one-sampling-time delay, which improves the estimation accuracy, especially when the sampling rate is low. The error compensation gain matrix L_c is obtained from the equation $L_p = \Phi L_c$. R. Miklosovic *et al* applied discrete pole location design and implemented the ESO in PE and CE forms in 2006, and named them as Predictive Discrete Extended State Observer (PDESO) and Current Discrete Extended State Observer (CDESO) respectively [14].

The pole location determination in the $\mathbf{z}$ domain for ESO becomes the solution of a discrete equation, $\lambda(\mathbf{z}) = |\mathbf{z}I - \Phi + L_p C| = (\mathbf{z} - \beta)^3$, where $\beta = e^{-\omega_o T}$. Thus the coefficient matrices of (2.16) in PDESO and CDESO under Euler and Zero-order-hold discretization methods are obtained, as shown in the following table.

Table I: PDESO and CDESO coefficient matrices

Type	Φ	Γ	L_p	L_c
Euler	$\begin{bmatrix} 1 & T & 0 \\ 0 & 1 & T \\ 0 & 0 & 1 \end{bmatrix}$	$\begin{bmatrix} 0 \\ bT \\ 0 \end{bmatrix}$	$\begin{bmatrix} 3(1-\beta) \\ 3(1-\beta)^2\frac{1}{T} \\ (1-\beta)^3\frac{1}{T^2} \end{bmatrix}$	$\begin{bmatrix} 1-\beta^3 \\ (1-\beta)^2(2+\beta)\frac{1}{T} \\ (1-\beta)^3\frac{1}{T^2} \end{bmatrix}$
ZOH	$\begin{bmatrix} 1 & T & \frac{T^2}{2} \\ 0 & 1 & T \\ 0 & 0 & 1 \end{bmatrix}$	$\begin{bmatrix} b\frac{T^2}{2} \\ bT \\ 0 \end{bmatrix}$	$\begin{bmatrix} 3(1-\beta) \\ 3(1-\beta)^2(\beta+5)\frac{1}{2T} \\ (1-\beta)^3\frac{1}{T^2} \end{bmatrix}$	$\begin{bmatrix} 1-\beta^3 \\ (1-\beta)^2(1+\beta)\frac{3}{2T} \\ (1-\beta)^3\frac{1}{T^2} \end{bmatrix}$

The discrete implementations of ADRC show the advantage of controller design in state space. The discrete pole location determination, the ZOH discretization, and the current estimator design in the state space are not available for the controllers designed in transfer function forms.

2.4 Other Disturbance Rejection Methods

2.4.1 Internal Model Control

IMC was the first method to estimate and compensate *external disturbances* in LTI system. It was developed in the late 1970s and widely used in chemical industries[4]. IMC is also the only one of the active disturbance rejection methods discussed in this thesis that was collected in *The Control Handbook* in 1996[5].

Structure

The 1-dof IMC structure is straightforward. Assume the real plant and its nominal model are $G_p(s)$ and $\hat{G}_p(s)$ respectively. The block diagram of the 1-dof IMC is shown in the following figure.

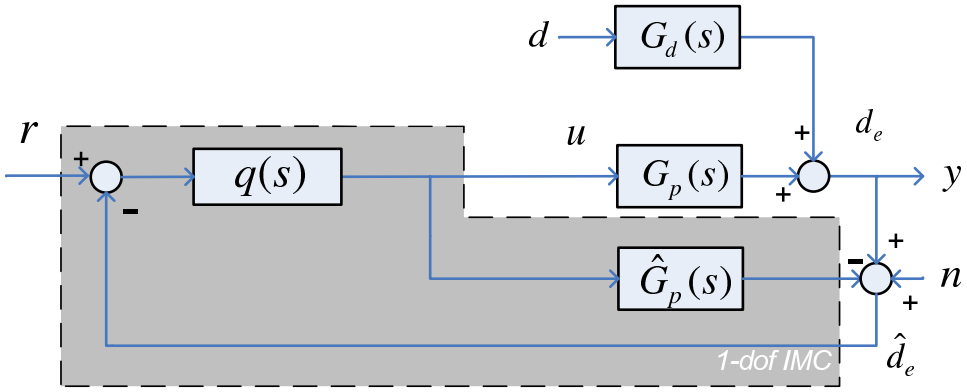

Figure 7: IMC diagram(1-dof)

As shown in Figure 7, the nominal plant model $\hat{G}_p(s)$ is constructed to obtain the nominal output from the control signal u. The difference between the measured real output and the nominal output is fed back to correct the control law. The transfer

functions of the system shown in Figure 7 are as follows.

$$\begin{aligned} G_{ry}(s) &= \frac{\hat{G}_p(s)q(s)}{1+\left(G_p(s)-\hat{G}_p(s)\right)q(s)} \\ G_{dy}(s) &= \frac{G_d(s)\left(1-\hat{G}_p(s)q(s)\right)}{1+\left(G_p(s)-\hat{G}_p(s)\right)q(s)} \end{aligned} \tag{2.18}$$

If $\hat{G}_p(s)$ matches $G_p(s)$, the denominators in (2.18) equals to 1. By choosing $q(s) = \frac{G_c(s)}{1+G_c(s)G_p(s)}$, this open-loop controller $q(s)$ acts as a closed-loop controller G_c with closed-loop transfer function of the system as $G_{ry}(s) = G_p(s)q(s) = \frac{G_c(s)G_p(s)}{1+G_c(s)G_p(s)}$.

The one-degree-of-freedom (1-dof) IMC structure is not flexible since only one controller is applied in the system. The disturbance rejection ability of this structure is also limited: when $G_p(s) = \hat{G}_p(s)$, the transfer function G_{dy} equals to $\frac{G_d(s)}{1+G_c(s)G_p(s)}$, which is same as a conventional closed-loop controller $G_c(s)$. Fortunately, the 1-dof IMC structure is easy to be extended to a 2-dof structure, which is shown as follows.

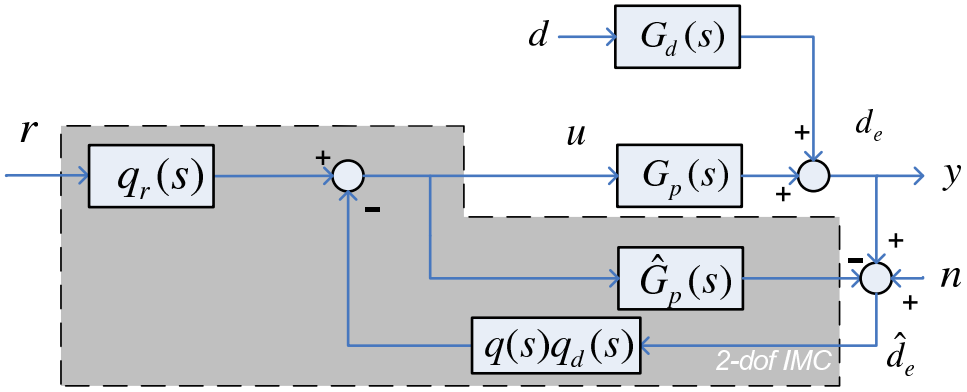

Figure 8: IMC diagram(2-dof)

From Figure 7 to Figure 8, only a simple block operation needs to be carried out: the controller $q(s)$ is moved ahead of the minus operator. Now there are two filters: one filters r and is called set-point filter and denoted as $q_r(s)$, and the other one is in the feedback loop and its notation remains as $q(s)$. A filter $q_d(s)$ is then

introduced into the feedback loop to make the structure 2-dof: $q_r(s)$ and $q(s)q_d(s)$. The transfer functions of the system in Figure 8 are as follows.

$$\begin{aligned} G_{ry}(s) &= \frac{\hat{G}_p(s)q(s)}{1+\left(G_p(s)-\hat{G}_p(s)\right)q(s)q_d(s)} \\ G_{dy}(s) &= \frac{\left(1-\hat{G}_p(s)q(s)q_d(s)\right)G_d(s)}{1+\left(G_p(s)-\hat{G}_p(s)\right)q(s)q_d(s)} \end{aligned} \tag{2.19}$$

Assuming there is no noise and $\hat{G}_p(s)$ matches $G_p(s)$, the denominators in (2.19) equal to 1. Then $q_r(s) = q(s)$ is designed as the one in the 1-dof IMC structure. The disturbance filter $q_d(s)$ is designed to get zeros to cancel the poles in $G_d(s)$ by solving $1 - \hat{G}_p(s)q(s)q_d(s) = 0$ at the poles of $G_d(s)$.

Feature

First, the whole method of IMC relies on the awareness of the plant model and the *external disturbances* model. As described in the section, the set-point filter and the disturbance rejection filter are designed specifically for a certain plant model. Otherwise, IMC cannot be applied. Second, the design of IMC itself is through transfer function derivation. Thus, IMC is only applicable in LTI environment. In addition, no rigorous stability proof is shown for IMC.

2.4.2 Unknown Input Observer

Direct *external disturbances* cancellation is a new idea which is quite different from IMC in design. UIO's idea comes from the disturbance feedforward described in Figure 3. Assuming the dynamics of the *external disturbances* are known, a fictitious state reconstructor is used in UIO to generate the estimation of the *external disturbances* from the input and the output information of the plant. This design of UIO

does not require the direct measurement of the disturbance, which is needed in the disturbance feedforward design.

The earliest direct *external disturbances* cancellation method is the Disturbance Accommodation Control (DAC) by C. D. Johnson in 1971 [20], which was later referred to by E. Schrijver as UIO. Later on, J. Profeta *et al* proposed a discrete version of UIO and showed some of its frequency responses[21]. Y. Guan *et al* applied reduced-order observer design in UIO in 1991[22].

Structure

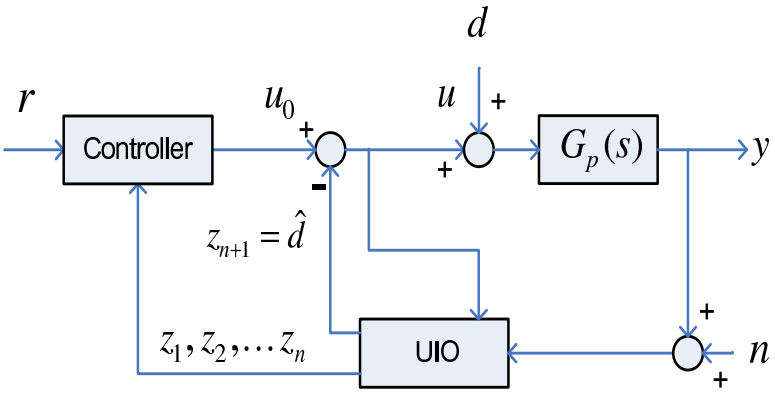

Figure 9: UIO diagram

Figure 9 shows the block diagram of UIO, where the plant is LTI, denoted as $G_p(s)$ and the UIO use the plant output and the control signal to estimate the *external disturbance*. The UIO form described in [23] is used here to easily illustrate the idea of UIO in order to make comparison between UIO and ESO easier in the next chapter. Assume that the models of the plant and the *external disturbances* are both known. The state space forms of the nominal plant model and the fictitious *external disturbances* reconstructor are presented in (2.20) and (2.21) respectively:

$$\begin{cases} \dot{x} = Ax + B(u + d) \\ y = Cx \end{cases} \tag{2.20}$$

where

$$A = \begin{bmatrix} 0 & 0 & \cdots & 0 & -a_0 \\ 1 & 0 & \cdots & 0 & -a_1 \\ \vdots & \vdots & \ddots & \vdots & \vdots \\ 0 & 0 & \cdots & 1 & -a_{n-1} \end{bmatrix}_{n\times n}, B = \begin{bmatrix} b_0 \\ \vdots \\ b_{n-1} \end{bmatrix}_{n\times 1}, C = \begin{bmatrix} 0 & \cdots & 0 & 1 \end{bmatrix}_{1\times n}$$

$$\begin{aligned} \dot{d} &= A_d d \\ \hat{d} &= C_d d \end{aligned} \tag{2.21}$$

where

$$A_d = \begin{bmatrix} 0 & 0 & \cdots & 0 & -q_0 \\ 1 & 0 & \cdots & 0 & -q_1 \\ \vdots & \vdots & \cdots & \vdots & \vdots \\ 0 & 0 & \cdots & 1 & -q_{h-1} \end{bmatrix}_{h\times h}, C_d = \begin{bmatrix} 0 & \cdots & 0 & 1 \end{bmatrix}_{1\times h}$$

With the states in (2.21) introduced, the state space model of the plant is augmented to the form in (2.22).

$$\begin{cases} \dot{x} = A_x x + B_x(u + d) \\ y = C_x x \end{cases} \tag{2.22}$$

where

$$A_x = \begin{bmatrix} A & BC_d \\ 0 & A_d \end{bmatrix}_{(n+h)\times(n+h)}, B_x = \begin{bmatrix} B \\ 0 \end{bmatrix}_{(n+h)\times 1}, C_x = \begin{bmatrix} C & 0 \end{bmatrix}_{1\times(n+h)}$$

Then an UIO is set up for the observation of states of the augmented plant, as shown in (2.23)

$$\dot{z} = A_z z + B_z u + LC_z(x - z) \tag{2.23}$$

where $A_z = A_x$, $B_z = B_x$, $C_z = C_x$, and L is an observer gain vector with $n + h$ elements designed to get the observer stable.

The estimated *external disturbance*, z_{n+h}, is then subtracted from the control signal to reject the real *external disturbances*. The estimated states(from z_1 to z_n) are then fed back for the control signal generation.

Features

Although designed in different way, UIO is the closest one to ESO among all the methods discussed in this research. Like ESO, the advantage of UIO is that, as a state observer, UIO estimates not only disturbances but also states. This is the benefit of ESO and UIO against DoB. With the estimation of the plant states, the control system with UIO is a state feedback control system.

The disadvantage of UIO is that, like IMC, UIO is constructed on the basis that the models of the plant and the disturbances are already known. Otherwise the method cannot be applied. Also, no stability proof is given for UIO applied to NTV systems.

2.4.3 Disturbance Observer

The idea of DoB is the input *external disturbances* estimation similar to UIO, but implemented in frequency domain as a transfer function design.

The original DoB was proposed by T. Umeno *et al* in 1991 as part of a parameterized linear 2-dof controller designed to reject *external disturbances* [24]. Here the equivalence between the 2-dof controller in the Type I system and some other disturbance observers, such as the disturbance torque observer developed by K. Ohishi *et al* in 1987[25], and the torque observer proposed by Y. Hori in 1988[26], are verified. The DoB design finally concentrates on the so-called Q-filter design.

Furthermore, in 1996, H. Lee *et al* applied DoB in the velocity loop together with a feedforward nonlinear friction compensator in high-speed motion control to

get better performance against nonlinear friction[27]; Cheng *et al* [28] and Yang *et al* [29] applied set-point feedforward along with DoB.

In 2002, E. Schrijver analyzed DoB (which is denoted as the Disturbance Estimating Filter (DEF) to be distinguished from UIO) in detail, disclosed the equivalence between UIO and DoB in the aspect of *external disturbances* estimation under certain conditions[23], and extended the application of DoB to non-minimum-phase plant. Schrijver speculated that, besides the *external disturbance* rejection function, DoB also presents the rejection ability against the discrepancy between the real plant and its nominal model in the low frequency. However, there is no proof for the this assertion.

Structure

With $G_p(s)$ and $\hat{G}_p(s)$ denoting the transfer functions of a real plant and its nominal model respectively, the block diagram of the *external disturbance* estimation and rejection of DoB is presented as follows.

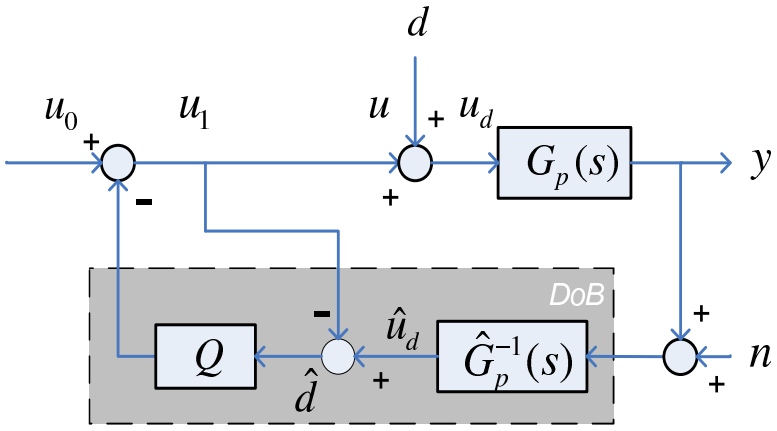

Figure 10: DoB disturbance rejection diagram

As shown in Figure 10, since the real plant $G_p(s)$ and its nominal model $\hat{G}_p(s)$ are not equal in the real world, the difference between the control inputs to them need to be estimated and rejected. The output of the real plant is fed back into the

inverse of the nominal plant to get the nominal control signal $\hat{u}_d$ that will generate the output in the nominal plant. Then $\hat{d}$, the estimation of *external disturbance* d, is obtained from the difference between u and $\hat{u}_d$ and cancelled in the control signal after a filter Q. Expressed in equation form, the *external disturbance* estimation of DoB is expressed in the following equation:

$$\hat{d} = Q\left(\hat{G}_p^{-1}(s)y(s) - u(s)\right) \tag{2.24}$$

There are three reasons to introduce Q into DoB. One is that direct feedback of $\hat{d}$ cannot be realized because normally the inverse plant is non-proper, which means the degree of the numerator is greater than the degree of the denominator. The filter Q in Figure 2.24 can be moved backwards before the subtraction operator. With $QG_p^{-1}(s)$ proper, DoB is then implementable. The second reason is that direct feedback would result in an algebraic loop. The last reason is that Q filter can filter the measurement noise in the feedback signal.

The transfer functions describing the relationship between input u_0, d, n, and output y in Figure 10 are as follows.

$$\begin{aligned} G_{u_0y}(s) &= \frac{G_p(s)\hat{G}_p(s)}{Q\left(G_p(s) - \hat{G}_p(s)\right) + \hat{G}_p(s)} \\ G_{dy}(s) &= \frac{G_p(s)\hat{G}_p(s)(1-Q)}{Q\left(G_p(s) - \hat{G}_p(s)\right) + \hat{G}_p(s)} \\ G_{ny}(s) &= -\frac{G_p(s)Q}{Q\left(G_p(s) - \hat{G}_p(s)\right) + \hat{G}_p(s)} \end{aligned} \tag{2.25}$$

The transfer functions in (2.25) show that the DoB structure effectively rejects disturbance in low frequency. However, at the same time measurement noise is introduced into the system through the disturbance rejection feedback. Therefore, the design of the Q filter is an essential part of DoB. The bandwidth of Q cannot be too high, which will introduce more noise. The bandwidth of Q can also not be too low,

which will degrade disturbance rejection performance. This trade-off also exists in all the other disturbance rejection methods.

In the 2-dof control method implemented with DoB, one dof is used as output feedback controller(which is the same as other controllers, such as PID), while the other(which is DoB) is used to estimate and reject the *external disturbance*, as shown in Figure 11.

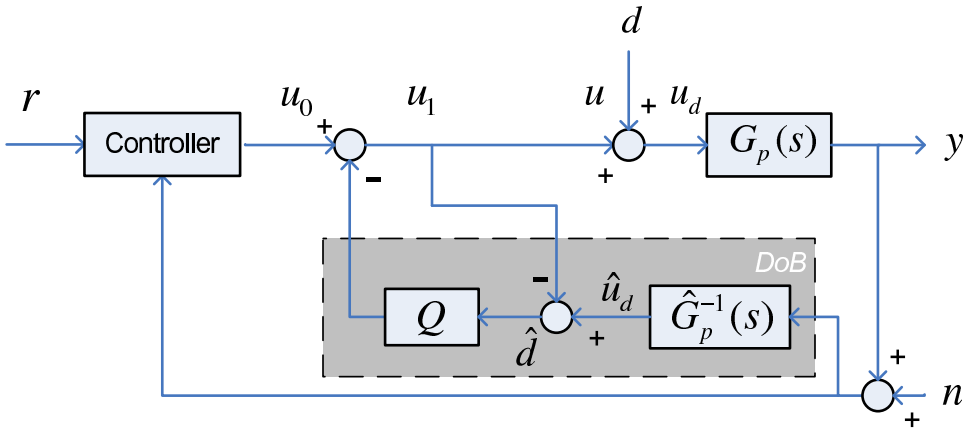

Figure 11: DoB diagram

DoB can also be interpreted in feedback loop, as shown in the following diagram.

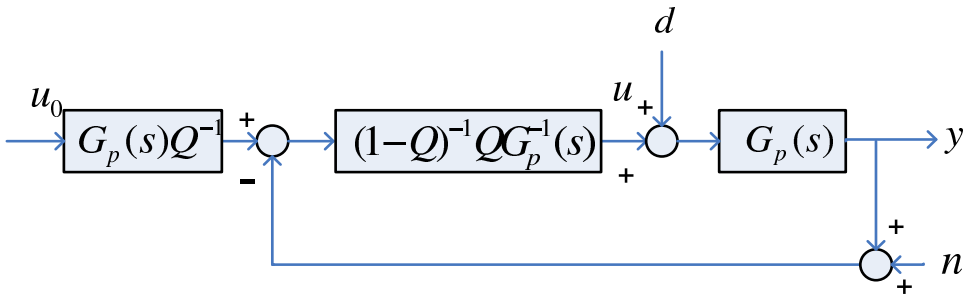

Figure 12: Feedback Interpretation of the DoB

Assume the plant is given as $G_p(s) = \frac{1}{ms}$ and the Q filter is designed as $\frac{1}{s\tau}$. The equivalent feedback controller $(1-Q)^{-1}QG_p^{-1}(s)$ is now a constant $\frac{m}{\tau}$. In this case the design of DoB is simplified to a proportional controller.

Features

DoB simplifies the *external disturbance* rejection design to a low-pass filter design, which makes it easy to understand. However, the explanation of how DoB works in Schrijver's work is kind of a contradiction. In the disturbance rejection explanation, Q needs to be approximately equal to 1 at low frequency to get the plant to act as the nominal plant. But in the feedback interpretation of DoB, as shown in Figure 12, Q cannot equal to one. Otherwise the system would have infinite gain which causes a singlarity in the system. Thus interpreting disturbance rejection in the form of Q may not be a good choice.

As a frequency-domain design method, DoB also has some other disadvantages. First, DoB requires that the nominal plant model and its inverse are available. If the detailed plant information is unknown, the inverse of it is not available and then the DoB method can not be applied. Second, DoB is designed for LTI systems only; therefore it cannot deal with nonlinearities. That is why the nonlinear friction compensation is introduced in [27]. Third, DoB can only estimate disturbance, which is determined by its control structure. Fourth, in order to implement DoB, the product $QG_p^{-1}(s)$ must proper. Thus Q normally needs to be designed as high-order low-pass filter and induce more phase lag into the system. Finally, except for the rigid body, there is no explicit stability proof for DoB. Schrijver also claimed that, although the nominal plant of DoB can be cascaded integrators, it is not recommended because "*for* $G_p(s) \neq \hat{G}_p(s)$*, stability and performance might be in danger*". This assertion shows that the nominal model need to be accurate in DoB.

2.4.4 Perturbation Observer

Several years after the appearance of DoB, the initial form of PoB was proposed together with a sliding mode controller as part of a tracking controller by S. Kwon

et al in 2001[30]. The concept of DoB is applied in the difference equation form to obtain disturbance estimation. In his work, S. Kwon *et al* applied three different PoBs(the Feedback Perturbation Observer (FBPO), the Feedforward Perturbation Observer (FFPO), and the Sliding Mode Perturbation Observer (SMPO)) in a parallel way, called the Multiloop Perturbation Compensation (MPEC) .

Getting an insight from the Time-Delayed Estimator (TDE), Kwon combined TDE and the filter design in DoB in 2003 to get the discrete realization of PoB[31]. The newest work of PoB is the combination of PoB and Kalman Filter in 2006 by Kwon[32].

Structure

PoB can be taken as a filtered version of TDE, or an implementation of DoB in the discrete time domain.

In TDE, the inverse of the plant model is obtained by a pseudoinverse algorithm. At the current time point, the states and control signal at the previous time point are used to estimate the *external disturbance* at the previous time point through the inverse plant model. Assume the disturbance remains the same during a sampling time period and then the current *external disturbance* estimation is obtained. PoB applies a Q filter(the low pass filter designed in DoB) on the *external disturbance* estimation obtained from TDE to get rid of noise in high frequency. Finally the filtered *external disturbance* estimation is rejected in the control signal.

Assume the discrete nominal plant model is the following equation.

$$\begin{cases} x(k+1) = \Phi x(k) + \Gamma(u(k) + d(k)) \\ y(k) = Cx(k) \end{cases} \tag{2.26}$$

Let Γ^+ denote the pseudoinverse of Γ. At k time point, $x(k)$, $x(k-1)$, and $u(k-1)$ are known and can be used to calculate the previous *external disturbance*

$d(k-1)$ through the inverse operation as shown in the following equation.

$$\hat{d}(k-1) = \Gamma^{+}\left(x(k) - \Phi x(k-1)\right) - u(k-1) \tag{2.27}$$

Assuming that the *external disturbance* changes little during $(k-1, k)$ time interval, $d(k) \approx d(k-1)$, a digital Q filter is applied to smooth $\hat{d}(k-1)$ and then $\hat{d}(k)$ is obtained.

$$\hat{d}(k) = Q\left(\Gamma^{+}\left(x(k) - \Phi x(k-1)\right) - u(k-1)\right) \tag{2.28}$$

The perturbation observer described in (2.28) is called FBPO. If the reference signals are used to replace the states in equation (2.28) under the assumption that the states track the reference closely, equation (2.28) is changed to FFPO.

Features

Since PoB can be looked on as implementation of DoB in discrete-time domain, this method has the same features as DoB except for that the *external disturbance* estimation and rejection is carried out in discrete-time, and that the discrete states of the system need to be available in PoB for the pseudoinverse operation.

2.4.5 Model Estimator

A PID Controller designed for the robust stabilization of SISO systems is proposed in 1994 by A. Tornambe *et al* [33]. Although the expression of this controller is quite different from DoB, UIO, or the other active disturbance rejection methods, it can estimate internal dynamics pretty well. To be distinguished from the other disturbance rejection methods, this controller is called ME in this thesis. Even though there is no *external disturbance* rejection declaration in ME, it has the ability to reject *external disturbance*.

Structure

ME deals with plants whose relative degree is equal to n(where the orders of the numerator and denominator of plant transfer function are q and p respectively and $n = p - q$). When expressed in state space, the plant model is the following equation.

$$\begin{cases} \dot{\epsilon} = A\epsilon + Bu \\ y = C\epsilon \end{cases} \tag{2.29}$$

Choose new states as the follows.

$$\begin{aligned} x_i &:= CA^{i-1}\epsilon, \quad i = 1, \cdots, n, \\ \eta_i &:= \epsilon_i, \qquad\quad i = 1, \cdots, p - n \end{aligned} \tag{2.30}$$

where x_i are observable states and η_i are unobservable states.

Then the plant model is simplified to

$$\begin{cases} \dot{x}_i = x_{i+1}, \quad i = 1, \cdots, n-1, \\ \dot{x}_n = f + u \\ y = x_1 \end{cases} \tag{2.31}$$

where $f = f(x_1, \cdots, x_{n-1}, \eta_1, \cdots, \eta_q, u)$ is the discrepancy between the simplified plant model and the desired model consisting of cascade integrators.

Assuming $x_n = y^{(n-1)}$ is available, an ME is constructed to get $\hat{f}$, the estimation of f, as shown in the following equation.

$$\begin{cases} \dot{\xi} = -l\xi - l^2 x_n - lu \\ \hat{f} = \xi + l x_n \end{cases} \tag{2.32}$$

where l is a low pass filter bandwidth.

As derived in the next section, the relative degree of the equivalent Q filter in ME equals one.

Features

ME is equivalent to one special case of RESO to be proposed in the next chapter. The advantage of ME is that, the observer has the minimum phase lag since the relative degree of the equivalent low pass filter is 1.

Although rigorous stability proof is provided for ME, it is under the assumption that the plant model is completely known. Another disadvantage of ME is that, its assumption that the up to $(n-1)^{th}$-order derivatives of the plant output are measurable is not realistic.

2.5 Comparisons of active disturbance rejection methods

2.5.1 Disturbance rejection diagram

From the diagram comparison among the different active disturbance estimation algorithms, a general diagram can be sketched out, as shown in Figure 13.

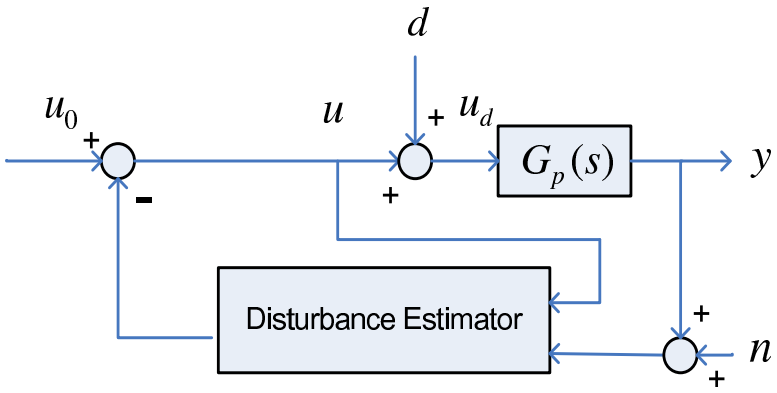

Figure 13: Diagram of general disturbance estimator

In all the algorithms discussed in this chapter, the control signal u and the system output y are used to estimate the disturbance, which is then rejected in the control signal.

2.5.2 Equation equivalence

IMC versus DoB

After a simple block diagram manipulation of Figure 10, the DoB diagram can be converted into following 2-dof IMC form. In the 2-dof IMC design in *Section 2.4.1*, one dof estimates and rejects disturbance, and the other one, as an open-loop controller, forces the output to follow the reference. Putting the open-loop controller aside, the disturbance rejection part of DoB is equivalent to that of IMC if $Q(s)\hat{G}_p^{-1}(s) = q(s)q_d(s)$.

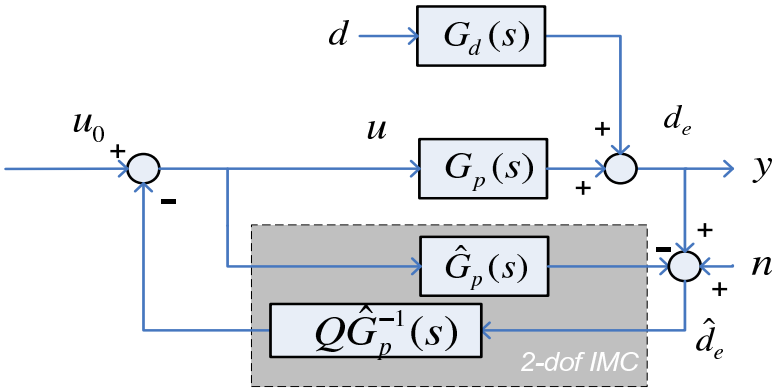

Figure 14: DoB in IMC form

ESO versus UIO and DoB

For UIO with the nominal plant as a set of cascade integrators , its state space form is identical to the form of ESO. This can be easily seen from the comparison between the ESO equation in (2.13) and the UIO equation in (2.23) when $n = 2$, $h = 2$ and the nominal plant of UIO is pure double integral plant (a_0, a_1, b_1 in (2.20) and q_0, q_1 in (2.21) all equal to zero).

The equivalence of DoB and UIO under certain conditions is already shown by Schrijver in [23]. Although DoB is not designed to estimate unknown dynamics, it is putted into the ESO framework for an n^{th}-order LTI plant to make comparison

between DoB and ESO. The differential equation of the LTI plant is as follows.

$$y^{(n)} + \sum_{i=0}^{n-1} a_i y^{(i)} = b(u+d) \tag{2.33}$$

The transfer function between u and y is $G_p(s) = \frac{b}{s^n + \sum_{i=0}^{n-1} a_i s^i}$. Defining $F(s) = -\sum_{i=0}^{n-1} a_i s^i$, which is assumed to be unknown and to be rejected, the transfer function of the plant can be written as $G_p(s) = \frac{b}{s^n - F(s)}$. The essence of ESO is to treat the plant as a series of cascade integraotrs no matter what it is. Therefore, assuming the nominal plant transfer function of DoB is $\hat{G}_p(s) = \frac{\hat{b}}{s^n}$, substituting $G_p(s)$, $\hat{G}_p(s)$ and $\rho = b/\hat{b}$ in equation (2.25), the transfer functions to be compared to ESO transfer functions in the next chapter are obtained, shown as follows.

$$\begin{aligned} G_{u_0 y}(s) &= \frac{\rho}{s^n + (1-Q)\rho s^n - (1-Q)F(s)} \\ G_{dy}(s) &= \frac{b(1-Q)}{s^n + (1-Q)\rho s^n - (1-Q)F(s)} = \hat{b}(1-Q)G_{u_0 y} \\ G_{ny}(s) &= -\frac{\rho s^n Q}{s^n + (1-Q)\rho s^n - (1-Q)F(s)} = -s^n Q G_{u_0 y} \end{aligned} \tag{2.34}$$

ME versus ESO and DoB

Substitute the second equation into the first equation in (2.32) and rearrange it to get $\dot{\hat{f}} = l(\dot{x}_n - u - \hat{f})$. Remember that the states $\dot{x}_{n-1}$ and $\dot{x}_n$ are defined as $y^{(n-1)}$ and $y^{(n)}$ respectively . Let $z = \hat{f}$. Substitute $\dot{x}_{n-1}$, $\dot{x}_n$, and z into the previous equation and get its Laplace form as follows.

$$Z(s) = \frac{l}{s+l}(s^n Y(s) - U(s)) \tag{2.35}$$

Compare (2.24) to (2.35), the two equations are the same when $Q(s) = \frac{l}{s+l}$ and $\hat{G}_p^{-1}(s) = s^n$. This derivation discloses that ME is equal to DoB when the nominal plant of DoB is cascaded integrators and the Q filter in DoB is designed as first order. Again, the nominal model of cascaded integrators is not suggested in DoB.

The equation (2.35) and the Laplace transform of the equation (3.5) are the same. Thus, ME is a special case of ESO when $y^{(n)}$ is available in ESO design, as shown in the next chapter.

2.5.3 General comparison

The overall comparison of different active disturbance rejection methods are shown in the following table. Among all the disturbance estimators in Table II, only ESO can deal with NTV plant. The NTV items are treated as a disturbance. IMC, DoB, UIO, PoB, and ME are based on the known linearized plant model. That is to say, these methods are applicable only near the equilibrium points where the plant is linearized. In [23], Schrijver mentioned that a DoB was applied to nonlinear plant in [34]. However, the nonlinearity of the plant is compensated by an Acceleration Tracking Controller, in which the nonlinearity is constructed based on the nonlinear plant model. Thus, in this nonlinear plant case, DoB only deals with the linear part of the plant.

Table II: Comparison of ADRC, IMC, DoB, UIO, PoB, and ME

	ESO	IMC	DoB	UIO	PoB	ME
Nonlinear TV support	Yes	No	No	No	No	No
Needed Model Information	Min	Max	Max	Max	Max	Min
State Estimation	Yes	No	No	Yes	No	Yes
Stability Proof on NTV system	Yes	Not	Available for special case	Not	Not	Yes

Among the discussed disturbance estimators, ESO and ME require the minimum plant information: the plant relative order n and the plant gain factor b. ADRC and ME achieve this by treating the internal plant dynamics as part of the distur-

bance and treating the plant as a series of cascade integrators. IMC, DoB, UIO and PoB need much more information: the nominal plant model. Real plants always contain nonlinearities. To implement these *model-based* disturbance algorithms, the real plants need to be linearized to get the approximated linear behavior of the plant near the equilibrium points. As a result, in DoB and PoB implementation, the inverse and the pseudo-inverse of the plant model need to be derived respectively, which adds much difficulty in their implementation.

As state observers, ESO and UIO estimate states besides the disturbance. Thus state feedback control methods can be applied with ESO or UIO. IMC, DoB, PoB, and ME merely estimate the disturbance. Therefore IMC, DoB, PoB, and ME can only be used with output feedback algorithms.

Finally, among these disturbance estimators, only ESO and ME have stability proofs. For ME, stability is not guaranteed except for the fact that the plant dynamics are given. The stability study of ESO goes further: not only the asymptotic stability proof for systems with known dynamics is provided; but also for systems with unknown dynamics, the estimation error and the closed-loop tracking error are shown to be bounded and have the inverse relationship with bandwidths of the observer and controller [17], [35].

CHAPTER III

REDUCED-ORDER EXTENDED STATE OBSERVER

The comparisons among different disturbance rejection methods in the previous chapter disclose an idea: disturbance rejection is of a common structure. That is, disturbance information obtained from the input and output data is manipulated and fed back into the control signal in real-time in a certain manner to reject disturbance. Under this common structure, the advantage of different methods can benefit each other. For example, the stability proof of ADRC can be utilized in the other methods. Another example is the filter design in DoB. This can also be used in the explanation of ESO and UIO. Indeed, observers work as low pass filters which decrease the measurement noise in the feedback loop. However, at the same time the low pass filters also bring phase lag. The bigger the relative order, the more the phase lag. Under this consideration, the equivalent first-order low pass filter in ME makes it attractive because it operates with the least phase lag compared to other methods. But this least phase lag is based on the assumption of ME that the $(n-1)^{th}$-order derivative

of the output is known. Therefore a question is raised: can we reduce the phase lag in ESO or UIO if the higher order derivative of the output signal is known? or in other words, can the order of the observer be reduced? This question natually leads to the reduced order observer.

In the rest of this chapter, first, RESOs are proposed to estimate the states and disturbance for a 2^{nd}-order plant. Then the ADRC with RESO is generalized for n^{th}-order plant. Finally the 2-dof transfer functions of the ADRC with RESO are derived to give some observations and to help the research on the frequency response analysis of ADRC.

3.1 Reduced-order Extended State Observer

The reduced-order observer was first introduced in 1964 by D.G. Luenberger [36]. The presumption of the reduced-order observer is that some of the plant outputs are known and do not need to be observed. The reduced-order observer under the condition that the derivatives of the system output are known was already discussed in Luenberger's work. In ADRC structure, application of reduced-order observer is straightforward. In the example in (2.3), the system output y is known through measurement and usually does not need to be estimated. The first derivative of y can be approximated from the difference of two neighboring y sample values divided by the sampling time, denoted as $\hat{\dot{y}}$. Thus, the reduced-order observer can by applied in ESO.

Before the proposal of RESO, the existing ESOs are reexamined to give some insights. The augmented plant model in (2.3) and the ESO in (2.4) are compared in

the following equations.

$$\dot{x}=\begin{bmatrix}0&1&0\\0&0&1\\0&0&0\end{bmatrix}x+\begin{bmatrix}0\\1\\0\end{bmatrix}bu+\begin{bmatrix}0\\0\\1\end{bmatrix}\dot{f} \qquad \begin{bmatrix}\dot{z}_1\\\dot{z}_2\\\dot{z}_3\end{bmatrix}=\begin{bmatrix}0&1&0\\0&0&1\\0&0&0\end{bmatrix}\begin{bmatrix}z_1\\z_2\\z_3\end{bmatrix}+\begin{bmatrix}0\\1\\0\end{bmatrix}\hat{b}u+\begin{bmatrix}l_1\\l_2\\l_3\end{bmatrix}(\hat{y}-z_1)$$
$$y=\begin{bmatrix}1&0&0\end{bmatrix}x \qquad \hat{f}=\begin{bmatrix}0&0&1\end{bmatrix}z \tag{3.1}$$

The blue shadow in (3.1) shows that the ESO matrices A_z and B_z are obtained from A_x and B_x directly. Since the 3^{rd}-order ESO in (3.1) contains the two original states x_1 and x_2, it is of full order.

Assuming $x_2 = \dot{y}$ is available, a RESO can be constructed with z_1 and z_2 estimating $x_2 = \dot{y}$ and $x_3 = f$, respectively. The relationship between the augmented plant state space model and the RESO is shown as follows.

$$\dot{x}=\begin{bmatrix}0&1&0\\0&0&1\\0&0&0\end{bmatrix}x+\begin{bmatrix}0\\1\\0\end{bmatrix}bu+\begin{bmatrix}0\\0\\1\end{bmatrix}\dot{f} \qquad \begin{bmatrix}\dot{z}_1\\\dot{z}_2\end{bmatrix}=\begin{bmatrix}0&1\\0&0\end{bmatrix}\begin{bmatrix}z_1\\z_2\end{bmatrix}+\begin{bmatrix}1\\0\end{bmatrix}\hat{b}u+\begin{bmatrix}l_1\\l_2\end{bmatrix}(\hat{y}-z_1)$$
$$y=\begin{bmatrix}1&0&0\end{bmatrix}x \qquad \hat{f}=\begin{bmatrix}0&1\end{bmatrix}z \tag{3.2}$$

As shown in (3.2), the RESO matrices A_z and B_z are obtained from the blue-shadowed part of A_x and B_x respectively. Thus the order of this RESO is 2, smaller than the order of the augmented plant model.

Here the observer equation is as follows:

$$\begin{cases} \dot{z} = A_z z + B_z u_1 + L(\dot{y} - C_z z) \\ \hat{f} = V z \end{cases} \tag{3.3}$$

where:

$$A_z = \begin{bmatrix} 0 & 1 \\ 0 & 0 \end{bmatrix}, B_z = \begin{bmatrix} 1 \\ 0 \end{bmatrix}, L = \begin{bmatrix} l_1 \\ l_2 \end{bmatrix}, C_z = [\ 1 \quad 0\ ], V = [\ 0 \quad 1\ ]$$

and $l_1 = 2\omega_o$, $l_2 = \omega_o^2$.

The order reduction in the RESO may be continued under the assumption that $\ddot{y}$ is available (which is equivalent to the assumption that the state $x_3 = \ddot{y} - bu$ is available). Another RESO can be constructed with z to track $x_3 = f$. The relationship between the augmented plant state space model and the new RESO is shown in the following equations.

$$\begin{aligned} \dot{x} &= \begin{bmatrix} 0 & 1 & 0 \\ 0 & 0 & 1 \\ 0 & 0 & 0 \end{bmatrix} x + \begin{bmatrix} 0 \\ 1 \\ 0 \end{bmatrix} bu + \begin{bmatrix} 0 \\ 0 \\ 1 \end{bmatrix} \dot{f} \qquad & \dot{z} &= [0] z + [0] \hat{b} u + [l]\left(\hat{\ddot{y}} - \hat{b} u - z\right) \\ y &= [1 \;\; 0 \;\; 0] x & \hat{f} &= z \end{aligned} \tag{3.4}$$

As shown in (3.4), the RESO matrices A_z and B_z are also obtained from the blue-shadowed part of A_x and B_x respectively. Thus the order of this RESO is 1. The difference between this RESO and the previous RESO is that the requirement changes from $x_2 = \dot{y}$ available to $x_3 = \ddot{y} - bu$ available. The RESO equation is as follows:

$$\begin{cases} \dot{z} = l(\ddot{y} - \hat{b}u - z) \\ \hat{f} = z \end{cases} \tag{3.5}$$

where $l = \omega_o$.

Define $\hat{f} = \xi + l\dot{y}$. Let $\hat{b} = 1$(The factor b is removed by its inverse in the control law in ME). Substitute $\hat{f}$ into (3.5) and get the same equations as the ones in (2.32). This demonstrates that ME is a special case of RESO.

The order reduction can also be applied when there are multiple extended states in the ESO, as shown in the following equations.

$$\begin{aligned} \dot{x} &= \begin{bmatrix} 0 & 1 & 0 & 0 \\ 0 & 0 & 1 & 0 \\ 0 & 0 & 0 & 1 \\ 0 & 0 & 0 & 0 \end{bmatrix} x + \begin{bmatrix} 0 \\ 1 \\ 0 \\ 0 \end{bmatrix} bu + \begin{bmatrix} 0 \\ 0 \\ 0 \\ 1 \end{bmatrix} \ddot{f} \qquad & \begin{bmatrix} \dot{z}_1 \\ \dot{z}_2 \\ \dot{z}_3 \\ \dot{z}_4 \end{bmatrix} &= \begin{bmatrix} 0 & 1 & 0 & 0 \\ 0 & 0 & 1 & 0 \\ 0 & 0 & 0 & 1 \\ 0 & 0 & 0 & 0 \end{bmatrix} \begin{bmatrix} z_1 \\ z_2 \\ z_3 \\ z_4 \end{bmatrix} + \begin{bmatrix} 0 \\ 1 \\ 0 \\ 0 \end{bmatrix} \hat{b} u + \begin{bmatrix} l_1 \\ l_2 \\ l_3 \\ l_4 \end{bmatrix} (\hat{y} - z_1) \\ y &= [1 \;\; 0 \;\; 0 \;\; 0] x & \hat{f} &= [0 \;\; 0 \;\; 1 \;\; 0] z \end{aligned} \tag{3.6}$$

$$\dot{x}=\begin{bmatrix}0&1&0&0\\0&0&1&0\\0&0&0&1\\0&0&0&0\end{bmatrix}x+\begin{bmatrix}0\\1\\0\\0\end{bmatrix}bu+\begin{bmatrix}0\\0\\0\\1\end{bmatrix}\ddot{f} \qquad \begin{bmatrix}\dot{z}_1\\\dot{z}_2\\\dot{z}_3\end{bmatrix}=\begin{bmatrix}0&1&0\\0&0&1\\0&0&0\end{bmatrix}\begin{bmatrix}z_1\\z_2\\z_3\end{bmatrix}+\begin{bmatrix}1\\0\\0\end{bmatrix}\hat{b}u+\begin{bmatrix}l_1\\l_2\\l_3\end{bmatrix}(\hat{y}-z_1)$$

$$y=\begin{bmatrix}1&0&0&0\end{bmatrix}x \qquad \hat{f}=\begin{bmatrix}0&0&1\end{bmatrix}z \tag{3.7}$$

$$\dot{x}=\begin{bmatrix}0&1&0&0\\0&0&1&0\\0&0&0&1\\0&0&0&0\end{bmatrix}x+\begin{bmatrix}0\\1\\0\\0\end{bmatrix}bu+\begin{bmatrix}0\\0\\0\\1\end{bmatrix}\ddot{f} \qquad \begin{bmatrix}\dot{z}_1\\\dot{z}_2\end{bmatrix}=\begin{bmatrix}0&1\\0&0\end{bmatrix}\begin{bmatrix}z_1\\z_2\end{bmatrix}+\begin{bmatrix}0\\0\end{bmatrix}\hat{b}u+\begin{bmatrix}l_1\\l_2\end{bmatrix}(\hat{\ddot{y}}-\hat{b}u-z_1)$$

$$y=\begin{bmatrix}1&0&0&0\end{bmatrix}x \qquad \hat{f}=\begin{bmatrix}0&1\end{bmatrix}z \tag{3.8}$$

As shown in (3.6), (3.7), and (3.8), the order of the ESO with two extended states reduces from 4 to 3, to 2 respectively.

3.2 Generalization of ADRC controller with RESO

A common framework of ADRC with RESO dealing with n^{th}-order plant is generalized in this chapter to facilitate analysis. The block diagram of the ADRC with RESO is shown as follows.

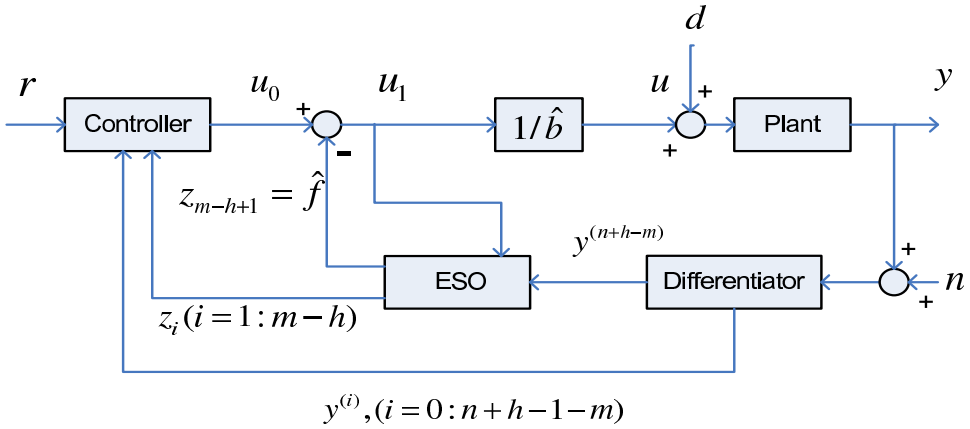

Figure 15: ADRC with Single-loop ESO Block Diagram

The plant in the Figure 15 is defined as an n^{th} order plant with differential

equation as follows.

$$y^{(n)} = f(y, \dot{y}, \cdots, d, t) + bu \tag{3.9}$$

where $f(y, \dot{y}, \cdots, d, t)$ denotes the *generalized disturbance* to be estimated and rejected.

Normally $\hat{b}$, the estimation of b, can be obtained. The influence of the ratio $\rho = b/\hat{b}$ on the system when it does not equal to 1 will be discussed later. Here assuming $\hat{b} = b$, a control law $u_1 = \hat{b}u$ is applied to remove the b factor influence from the system. Thus, with u_1 as input and y as output, equation(3.9) becomes the unity gain plant, shown as follows.

$$y^{(n)} = f(y, \dot{y}, \cdots, d, t) + u_1 \tag{3.10}$$

Choose states as $x_1{=}y$, $x_2{=}\dot{x}_1{=}\dot{y}$, $\cdots$, $x_n{=}\dot{x}_{n-1}{=}y^{(n-1)}$. Also choose h extended states as $x_{n+1}{=}f$, $x_{n+2}{=}\dot{x}_{n+1}{=}\dot{f}$, $\cdots$, $x_{n+h}{=}\dot{x}_{n+h-1}{=}f^{(h-1)}$. The unity gain plant (3.10) can now be expressed in the augmented matrix

$$\begin{bmatrix} \dot{x}_1 \\ \dot{x}_2 \\ \vdots \\ \dot{x}_{n+l-m} \\ \dot{x}_{n+l-m+1} \\ \vdots \\ \dot{x}_n \\ \dot{x}_{n+1} \\ \vdots \\ \dot{x}_{n+h} \end{bmatrix} = \begin{bmatrix} 0 & 1 & 0 & 0 & 0 & \ddots & 0 & 0 & 0 & 0 \\ 0 & 0 & \ddots & 0 & \ddots & \ddots & \ddots & \ddots & \ddots & 0 \\ \vdots & \ddots & \ddots & 1 & 0 & \ddots & \ddots & \ddots & \ddots & \vdots \\ 0 & 0 & \ddots & 0 & 1 & 0 & \ddots & \ddots & \ddots & 0 \\ 0 & \ddots & \ddots & \ddots & 0 & 1 & 0 & \ddots & \ddots & 0 \\ \vdots & \ddots & \ddots & \ddots & 0 & 0 & 1 & 0 & \ddots & \vdots \\ 0 & \ddots & \ddots & \ddots & \ddots & \ddots & 0 & 1 & \ddots & 0 \\ 0 & \ddots & \ddots & \ddots & \ddots & \ddots & \ddots & 0 & \ddots & 0 \\ \vdots & \ddots & \ddots & \ddots & \ddots & \ddots & \ddots & \ddots & \ddots & 1 \\ 0 & 0 & 0 & 0 & 0 & 0 & 0 & 0 & 0 & 0 \end{bmatrix} \begin{bmatrix} x_1 \\ x_2 \\ \vdots \\ x_{n+l-m} \\ x_{n+l-m+1} \\ \vdots \\ x_n \\ x_{n+1} \\ \vdots \\ x_{n+h} \end{bmatrix} + \begin{bmatrix} 0 \\ \vdots \\ 0 \\ \vdots \\ 0 \\ 1 \\ 0 \\ \vdots \\ 0 \end{bmatrix} u_1 + \begin{bmatrix} 0 \\ \vdots \\ \vdots \\ \vdots \\ \vdots \\ \vdots \\ \vdots \\ 0 \\ 1 \end{bmatrix} f^{(h)} \tag{3.11}$$

or in state space form

$$\begin{cases} \dot{x} = A_x x + B_x u_1 + E f^{(h)} \\ y = C_x x \end{cases} \tag{3.12}$$

where

$$A_x = \begin{bmatrix} 0 & 1 & 0 & \cdots & 0 \\ 0 & 0 & 1 & \cdots & 0 \\ 0 & 0 & 0 & \ddots & \vdots \\ \vdots & \vdots & \ddots & \ddots & 1 \\ 0 & 0 & 0 & \cdots & 0 \end{bmatrix}_{(n+h)\times(n+h)}, B_x = \begin{bmatrix} 0 \\ \vdots \\ 0 \\ 1 \\ 0 \\ \vdots \\ 0 \end{bmatrix}_{(n+h)\times 1}, E = \begin{bmatrix} 0 \\ \vdots \\ 0 \\ 1 \end{bmatrix}_{(n+h)\times 1}$$

$$C_x = [\ 1 \quad 0 \quad \cdots \quad 0\ ]_{1\times(n+h)}$$

where the nonzero element in B_x is in the n^{th} row.

Assume y, $\dot{y}$, $\cdots$, $y^{(n+h-m)}$are available. Then the states x_1, x_2, $\cdots$, $x_{n+h-m+1}$ are available (If m=h, the last state can be obtained from its definition: $x_{n+1} = f = y^{(n)} - u_1$). Also assume $f^{(h)}$ does not change rapidly and can be ignored. According to the reduced-order observer design in the previous chapter, ESO order can be reduced to m, where $h \le m \le n + h$. Apply the order reduction operation in the same way as the previous section and get the ESO as follows.

$$\begin{bmatrix} \dot{z}_1 \\ \vdots \\ \dot{z}_{m-h} \\ \dot{z}_{m-h+1} \\ \vdots \\ \dot{z}_m \end{bmatrix} = \begin{bmatrix} 0 & 1 & 0 & \cdots & \cdots & 0 \\ \vdots & \ddots & 1 & \ddots & \ddots & \\ 0 & \ddots & \ddots & \ddots & \ddots & 0 \\ 0 & \ddots & \ddots & \ddots & \ddots & 0 \\ \vdots & \ddots & \ddots & \ddots & \ddots & 1 \\ 0 & 0 & \cdots & \cdots & \cdots & 0 \end{bmatrix} \begin{bmatrix} z_1 \\ \vdots \\ z_{m-h} \\ z_{m-h+1} \\ \vdots \\ z_m \end{bmatrix} + \begin{bmatrix} 0 \\ \vdots \\ 1 \\ 0 \\ \vdots \\ 0 \end{bmatrix} u_1 + \begin{bmatrix} l_1 \\ \vdots \\ l_{m-h} \\ l_{m-h+1} \\ \vdots \\ l_m \end{bmatrix} (x_{n+h-m+1} - z_1)$$

$$\hat{f} = [0 \ \cdots \ 0 \ 1 \ \cdots \ 0]z \tag{3.13}$$

Now z_1, $\cdots$, z_m are designed to estimate $x_{n+h-m+1}$, $\cdots$, x_{n+h}, respectively. The shadowed gain matrices in the ESO are obtained from the matrices of the augmented plant directly. For tuning simplicity, the observer gains l_1, $\cdots$, l_m are chosen as

$l_i = \begin{pmatrix} m \\ i \end{pmatrix} \omega_o^i$ where $0 < i \leq m$. $\begin{pmatrix} m \\ i \end{pmatrix}$ denotes the Binomial Coefficient $\frac{m!}{i!(m-i)!}$.

Also, to make the transfer function derivation easier, define $l_0 = \begin{pmatrix} m \\ 0 \end{pmatrix} \omega_o^0 = 1$.

Equation (3.13) is also expressed as follows.

$$\begin{cases} \dot{z} = A_z z + B_z u_1 + L\left(x_{n+h-m+1} - C_z z\right) \\ \hat{f} = Vz \end{cases} \tag{3.14}$$

where

$$A_z = \begin{bmatrix} 0 & 1 & 0 & \cdots & 0 \\ 0 & 0 & 1 & \cdots & 0 \\ 0 & 0 & 0 & \ddots & \vdots \\ \vdots & \vdots & \ddots & \ddots & 1 \\ 0 & 0 & 0 & \cdots & 0 \end{bmatrix}_{m \times m}, L = \begin{bmatrix} l_1 \\ l_2 \\ \vdots \\ l_m \end{bmatrix}_{m \times 1},$$

$$C_z = \begin{bmatrix} 1 & 0 & \cdots & \cdots & 0 \end{bmatrix}_{1 \times m}$$

if $m = h$,

$$B_z = [0]_{m \times 1}, V = \begin{bmatrix} 1 \\ 0 \\ \vdots \\ 0 \end{bmatrix}_{m \times 1};$$

if $m > h$,

$$B_z = \begin{bmatrix} 0 \\ \vdots \\ 0 \\ 1 \\ 0 \\ \vdots \\ 0 \end{bmatrix}_{m \times 1}, V = \begin{bmatrix} 0 \\ \vdots \\ 0 \\ 1 \\ 0 \\ \vdots \\ 0 \end{bmatrix}_{m \times 1}$$

(when $m > h$, the nonzero elements of B_z and V are in the $(m-h)^{th}$ row and $(m-h+1)^{th}$ row respectively.)

When $m = n+h$, the ESO is of full order and estimates all the states $x_1, \cdots, x_n$, the disturbance f and its derivatives; when $h < m < n+h$, ESO estimates the states $x_{n+h-m+1}, \cdots, x_n$, f and its derivatives; when $m = h$, the ESO is of the least order and estimates only f and its derivatives.

With the state z_{m-h+1} in the ESO to estimate f, a control law, $u_1 = u_0 - z_{m-h+1}$, is applied to reduce the plant to a pure n^{th} order plant $y^{(n)} = u_0$.

Then a parameterized general PD control law is applied to control the pure n^{th} order plant as follows.

$$u_0 = \sum_{i=1}^{n+1} k_i r^{(i-1)} - \sum_{i=1}^{n+h-m} k_i y^{(i-1)} - \sum_{i=1}^{m-h} k_{n+h-m+i} z_i \tag{3.15}$$

where $k_i = \begin{pmatrix} n \\ i-1 \end{pmatrix} \omega_c^{n+1-i}$, $1 \le i \le n+1$, and the item $\sum_{i=1}^{n+h-m} k_i$ does not exit when $m = n+h$ because all the feedback signals come from ESO output under this condition.

3.3 Transfer Function Derivation

To analyze the ADRC in the frequency domain, the plant is narrowed to a LTI system. Although this degradation hides some advantages of ADRC, such as the ability to deal with nonlinear plant and the efficiency when the control law and the ESO in ADRC are designed with nonlinear gains, the analysis will still give insights of how ADRC works.

Suppose the plant is a n^{th}-order LTI system with differential equation as the follows.

$$y^{(n)} + \sum_{i=0}^{n-1} a_i y^{(i)} = bu \tag{3.16}$$

where a_i, $i = 0 : n-1$ and b are constant coefficients.

As shown in Figure 15, an external disturbance d is introduced into the plant. Thus, the disturbed plant differential equation of (3.16) is as the follows.

$$y^{(n)} + \sum_{i=0}^{n-1} a_i y^{(i)} = b(u+d) \tag{3.17}$$

Define $\hat{b}$ as the estimation of b and apply $u = u_1/\hat{b}$ in (3.17)to get

$$y^{(n)} = u_1 - \sum_{i=0}^{n-1} a_i y^{(i)} + (\rho - 1)u_1 + bd \tag{3.18}$$

where ρ is the ratio between real plant parameter b and it's estimation, $\rho = b/\hat{b}$.

The goal of disturbance rejection is to estimate the dynamics and disturbance besides $y^{(n)} = u$. Let $f = -\sum_{i=0}^{n-1} a_i y^{(i)} + (\rho - 1)u_1 + bd$ denote the *generalized disturbance*. Define $F(s) = -\sum_{i=0}^{n-1} a_i s^{i-1}$. Thus the Laplace transform of the *generalized disturbance* f can be expressed as $\mathcal{L}\{f\} = F(s)Y(s) + (\rho - 1)U_1(s) + bD(s)$, and the Laplace transform of (3.17) is expressed as follows.

$$s^n Y(s) = F(s)Y(s) + U_1(s) + (\rho - 1)U_1(s) + bD(s) \tag{3.19}$$

Furthermore, the Laplace Transform of the states are also expressed in vector form

$$X(s) = \begin{bmatrix} X_1(s) \\ X_2(s) \\ \vdots \\ X_n(s) \\ X_{n+1}(s) \\ X_{n+2}(s) \\ \vdots \\ X_{n+h}(s) \end{bmatrix} = \begin{bmatrix} 1 \\ s \\ \vdots \\ s^{n-1} \\ F(s) \\ sF(s) \\ \vdots \\ s^{h-1}F(s) \end{bmatrix} Y(s) + \begin{bmatrix} 0 \\ 0 \\ \vdots \\ 0 \\ 1 \\ s \\ \vdots \\ s^{h-1} \end{bmatrix} ((\rho - 1)U_1(s) + D(s)) \tag{3.20}$$

3.3.1 Procedure

To minimize the derivation work, the transfer functions needed in analysis are derived in the following steps.

Compensated plant transfer function

The whole system is divided into two parts with respect to u_0 and y. the part of the system that between u_0 and y, denoted as $G_{p0}(s)$, is the approximated cascade integrators(after disturbance estimation and rejection), as shown in Figure 16.

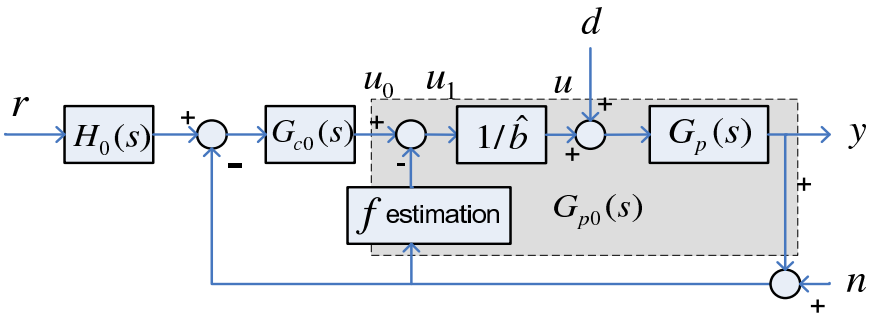

Figure 16: Compensated plant Block Diagram

The noise n introduced by disturbance rejection and the disturbance d are derived to act on u_0 with transfer functions $G_n(s)$ and $G_d(s)$ respectively, as shown in Figure 17.

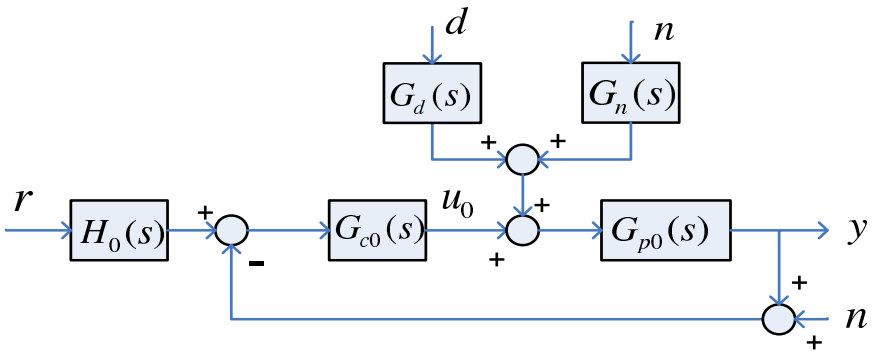

Figure 17: 2-dof (U_0) Block Diagram

2-dof transfer function with respect to u_0

The rest of the plant is then fit into a 2-dof control structure with r and y as inputs and u_0 as output, the two transfer functions in which are $H_0(s)$ and $G_{c0}(s)$ respectively, as shown in Figure 17.

2-dof transfer function with respect to u

Then from Figure 16, the disturbance rejection part and the scaling factor $1/\hat{b}$ are included into the control part and then $H(s)$ and $G_c(s)$, the transfer functions in 2-dof control structure with respect to u and y, are obtained, as shown in Figure 18.

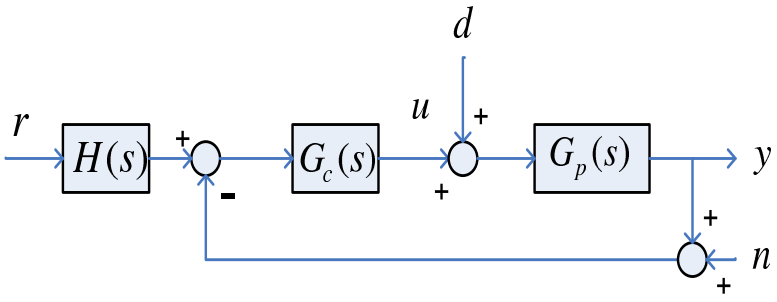

Figure 18: 2-dof (U) Block Diagram

3.3.2 Results

The detail derivation of the transfer functions are presented in *Appendix A*. Here only the derivation results are shown.

Define $Q = \frac{\Psi^m_{m-h+1,m}}{\Psi^m_{0,m}}$(the defination of Ψ is in the begining part of *Appendix A*), which is consistent with the Q filter in DoB and makes the comparison between DoB and ADRC easier. Substitute Q into (A.24) and get the following equation.

$$Y(s) = \frac{\rho U_0(s) + (1-Q)bD(s) - \rho Q s^n N(s)}{s^n + (\rho - 1)s^n Q - F(s)(1-Q)} \tag{3.21}$$

From (3.21), the transfer functions in Figure 17 are obtained, as the follows.

$$\begin{aligned} G_{p0}(s) &= \frac{\rho}{s^n + (\rho-1)s^n Q - F(s)(1-Q)} \\ G_d(s) &= \hat{b}(1-Q) \\ G_n(s) &= -Qs^n \end{aligned} \tag{3.22}$$

The 2-dof transfer functions $H_0(s)$, $G_{c0}(s)$, $H(s)$, and $G_c(s)$ are shown in (A.33), (A.32), (A.37), and (A.36), respectively in Appendix A.

3.3.3 Analysis

Q filter design mapping

Transfer functions in (3.22) are in the same form as (2.34) . Thus, the mapping between ADRC RESO design and DoB Q-filter design in disturbance rejection aspect can be established when nominal plant of DoB is cascade integrators, as shown in the following table.

Table III: Mapping between DoB and parameterized ESO

DoB	ESO	DoB	ESO
Q_{30}	m=3, h=1	Q_{20}	m=2, h=1
Q_{31}	m=3, h=2	Q_{21}	m=2, h=2
Q_{32}	m=3, h=3	Q_{10}	m=1, h=1

States and Disturbance Estimation

In the low frequency, $\frac{\Psi^m_{i,m}}{\Psi^m_{0,m}} \approx 1$, where $0 < i \leq m$; $\frac{\Psi^m_{i,j}}{\Psi^m_{0,m}} \approx 0$, where $0 \leq i < m$ and $0 \leq j < m$. Also, measurement noise can be ignored in low frequency. Substitute

these approximated equations into (A.28) and (A.29) and get the follows.

$$Z(s) = \frac{\begin{bmatrix} s^{n+h-m}\rho \\ \vdots \\ s^{n+h-1+w-m}\rho \\ \vdots \\ s^{n-1}\rho \\ s^n(\rho-1)+F(s) \\ \vdots \\ s^{n+h-1+w-m}(\rho-1)+F(s)s^{h-1+w-m} \\ \vdots \\ s^{n+h-1}(\rho-1)+F(s)s^{h-1} \end{bmatrix} U_0(s) \begin{bmatrix} 0 \\ \vdots \\ 0 \\ \vdots \\ 0 \\ s^n \\ \vdots \\ s^{n+h-1+w-m} \\ \vdots \\ s^{n+h-1} \end{bmatrix} bD_i(s)}{\rho s^n} \tag{3.23}$$

$$X(s) = \frac{\begin{bmatrix} \rho \\ \vdots \\ \rho s^{w-1} \\ \vdots \\ \rho s^{n-1} \\ s^{(n+1)-1}(\rho-1)+s^{(n+1)-1-n}F(s) \\ \vdots \\ s^{w-1}(\rho-1)+s^{w-1-n}F(s) \\ \vdots \\ s^{(n+h)-1}(\rho-1)+s^{(n+h)-1-n}F(s) \end{bmatrix} U_0(s)+ \begin{bmatrix} 0 \\ \vdots \\ 0 \\ \vdots \\ 0 \\ s^{(n+1)-1} \\ \vdots \\ s^{w-1} \\ \vdots \\ s^{(n+h)-1} \end{bmatrix} bD_i(s)}{\rho s^n} \tag{3.24}$$

where w denotes the row number of the vector.

Equation (3.24) shows that, in the low frequency, $z_1, \cdots, z_m$ can track the states $x_{n+h-m+1}, \cdots, x_{n+h}$ respectively.

Controller Type and Phase Lag

The equivalent 2-dof controller transfer functions of ADRC with RESO (the same as (A.38)) are as follows.

$$G_c(s) = \frac{1}{\hat{b}} \frac{\Psi_{0,m}^m \sum_{j=1}^{n+h-m} k_j s^{(j-1)} + \sum_{j=1}^{m-h+1} k_{n+h-m+j} s^{n+h-1-m+j} \Psi_{j,m}^m}{\sum_{j=1}^{m-h+1} k_{n+h-m+j} s^{h-1+j-m} \Psi_{0,j-1}^m}$$

$$H(s) = \frac{\Psi_{0,m}^m \sum_{j=1}^{n+1} k_j s^{(j-1)}}{\Psi_{0,m}^m \sum_{j=1}^{n+h-m} k_j s^{(j-1)} + \sum_{j=1}^{m-h+1} k_{n+h-m+j} s^{n+h-1-m+j} \Psi_{j,m}^m}$$

where $1 \leq h$, $h \leq m \leq n+h$, and $\sum_{i=1}^{n+h-m} k_i s^{(i-1)} = 0$ when $m = n+h$.

The highest order of the numerator in $G_c(s)$ is $n+h-1$. When $m = n+h$, the lowest order of the numerator in $G_c(s)$ is determined by its second item and equals 0; when $m < n+h$, the lowest order of the numerator in $G_c(s)$ is determined by its first item and equal to 0. The highest order and the lowest order of the denominator in $G_c(s)$ are m and h respectively. Therefore, $G_c(s)$ can be expressed as follows.

$$G_c(s) = \frac{\sum_{i=0}^{n+h-1} c_{ni} s^i}{\sum_{i=h}^{m} c_{di} s^i} \tag{3.25}$$

where c_{ni} and c_{di} are constants.

Equation (3.25) shows that the relative degree of the $G_c(s)$ is $n+h-m-1$. When m decreases, the phase lag decreases. It also can be concluded that this controller contributes h integrators to the open-loop transfer function.

Similarly, $H(s)$ can be expressed as follows.

$$H(s) = \frac{\sum_{i=0}^{n+m} c_{ni} s^i}{\sum_{i=0}^{n+h-1} c_{di} s^i} \tag{3.26}$$

where c_{ni} and c_{di} are constants, different from the ones in (3.25).

CHAPTER IV

FREQUENCY RESPONSE ANALYSIS OF ADRC

In this thesis, for simplicity, only ADRC controllers with one-extended-state ESO or RESO , which are applied on a linear time-invariant second-order plant, are analyzed. The differential equation and the transfer function of the studied plant are as follows:

$$\ddot{y} = -a_1\dot{y} - a_0 y + b(u + d) \tag{4.1}$$

where a_0 and a_1 are unknown.

$$G_p(s) = \frac{b}{s^2 + a_1 s + a_0} \tag{4.2}$$

Since both the plant and the controller are linear, the robustness of the control system can be evaluated using frequency response.

Consider a particular motion control example, where the plant in (4.1) comes with the parameters of $a_0 = 0$, $a_1 = 3.085$ and $b = 206.25$, and a particular ADRC designed with $\omega_o = \omega_c = 100$ rad/sec.

Three tasks will be carried out for each ADRC controller in the following analysis. First, with $\hat{b} = b = 206.25$, the stability boundaries of plant uncertainty coefficients a_0 and a_1 for different ADRC control bandwidth are investigated. This task is to show the plant uncertainty range within which the ADRC controller can keep the system stable. Second, when the ADRC controller is fixed, the uncertainty coefficients a_0 and a_1 are changed to investigate the stability margins. This task is to verify the ability of ADRC to reject parametric uncertainties. The influence of the ratio ρ between b and $\hat{b}$ are also studied. Finally, with the uncertainty coefficient a_0 and a_1 varying, the input disturbance sensitivity transfer function is investigated to show the robustness of ADRC on external disturbance rejection.

Since the main difference between ESO and RESO is the observer order, the analysis is focus on ADRC with ESO, while ADRC with RESO controllers are discussed in the later section.

4.1 ADRC with ESO

The original ADRC controller, as described in *Section 2.3.1*, is inspected in this section. If ADRC indeed estimates f and cancels it out, then we should see very little change in bandwidth and stability margins when a_0 and a_1 vary. To verify this prediction in the frequency response, the 2-dof transfer functions, denoted by $G_{c3}(s)$ and $H_3(s)$, are obtained from (A.36) and (A.37) respectively, as shown in the following equations.

$$\begin{aligned} G_{c3}(s) &= \frac{1}{\hat{b}} \frac{(3\omega_c^2\omega_o + 6\omega_c\omega_o^2 + \omega_o^3)s^2 + (3\omega_c^2\omega_o^2 + 2\omega_c\omega_o^3)s + \omega_c^2\omega_o^3}{s(s^2 + (2\omega_c + 3\omega_o)s + \omega_c^2 + 6\omega_c\omega_o + 3\omega_o^2)} \\ H_3(s) &= \frac{(s^3 + 3\omega_o s^2 + 3\omega_o^2 s + \omega_o^3)(s^2 + 2\omega_c s + \omega_c^2)}{(3\omega_c^2\omega_o + 6\omega_c\omega_o^2 + \omega_o^3)s^2 + (3\omega_c^2\omega_o^2 + 2\omega_c\omega_o^3)s + \omega_c^2\omega_o^3} \end{aligned} \tag{4.3}$$

(4.4)

From these transfer functions, the loop gain transfer function $G_{lg}(s)$, the closed-

loop system transfer function $G_{ry}(s)$, and the input disturbance sensitivity transfer function $G_{dy}(s)$ are readily available as follows.

$$G_{lg}(s) = G_p(s)G_c(s) \tag{4.5}$$

$$G_{ry}(s) = \frac{Y(s)}{R(s)} = \frac{H(s)G_c(s)G_p(s)}{1 + G_c(s)G_p(s)} \tag{4.6}$$

$$G_{dy}(s) = \frac{G_p(s)}{1 + G_c(s)G_p(s)} \tag{4.7}$$

4.1.1 Bandwidth and Stability

The stability of a closed-loop transfer function is determined by the pole locations of (4.6). Since $H(s)$ is guaranteed stable, because all three coefficients in their denominator are positive, the closed-loop stability can be determined from the poles of $\frac{G_c(s)G_p(s)}{1+G_c(s)G_p(s)}$. The question is, given a controller with fixed $\omega_o = \omega_c$, in what range of a_0 and a_1 the closed-loop system is stable?

Finding the analytical solution using Routh-Hurwitz criterion is too complex for this problem. Instead, a search program is used to determine the region in a_0-a_1 plane where the closed-loop system is stable. And this is repeated for different $\omega_o = \omega_c$. The results are shown in Figure 19, where the area to the upper-right side of the curve is the stable region.

Figure 19 shows that as the bandwidth, $\omega_o = \omega_c$, increases, the stable area in a_0-a_1 plane is expanded, particularly to the left on the a_0 axis. It also shows that even if the plant is unstable (either a_0 or a_1 is negative), the closed-loop system can still be made stable, given enough controller and observer bandwidth. In other words, the higher the bandwidth, the more parametric uncertainties the system can tolerate.

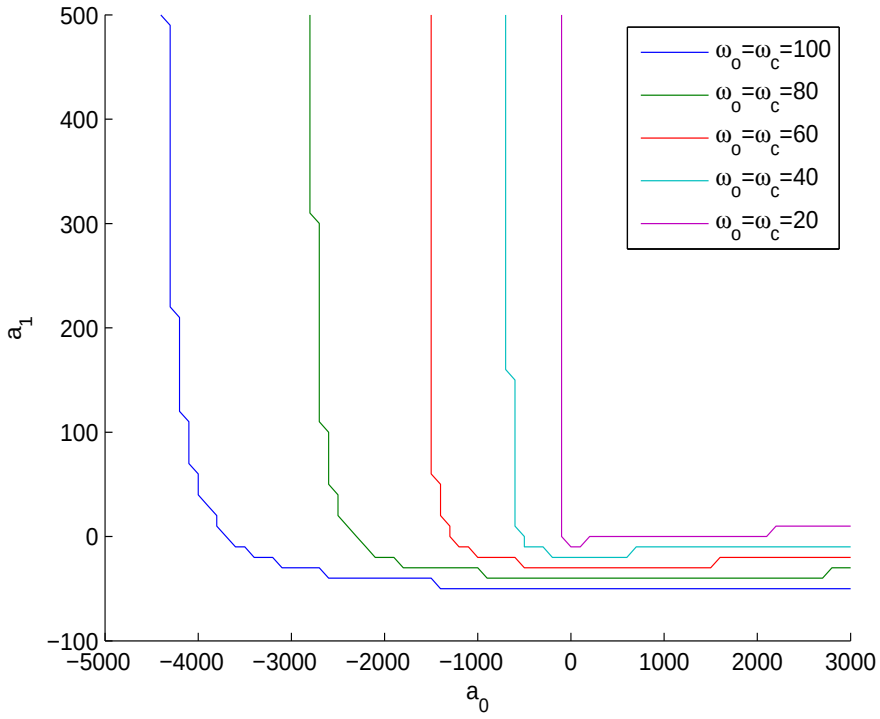

Figure 19: Stability of ADRC in a_0-a_1 plane (3^{rd}-order ESO)

4.1.2 Loop Gain Frequency Response

The Bode plots of the loop gain transfer function are shown in Fig.20, with $\omega_c = \omega_o = 100$ rad/sec, $b = 206.25$, $a_1 = 3.085$, and $a_0 = [0, 0.1, 1, 10, 100]$. The stability margin for each curve in Figure 20 is shown in Table IV. Figure 20 and Table IV show that, remarkably, gain margin, phase margin and cross-over frequency are almost immune to the changes in a_0.

Table IV: Gain Margin and Phase margin under different a_0 (3^{rd}-order ESO)

	neg GM dB (rad/sec)	pos GM	PM deg(rad/sec)
a0=0	-13.0 (34)	11.7 (276)	33.7 (100)
a0=0.1	-13.0 (34)	11.7 (276)	33.7 (100)
a0=1	-12.9 (34)	11.7 (276)	33.7 (100)
a0=10	-13.1 (34)	11.7 (276)	33.7 (100)
a0=100	-13.9 (33)	11.7 (276)	33.7 (101)

Similarly, the Bode plots of the loop gain transfer function are shown on Figure

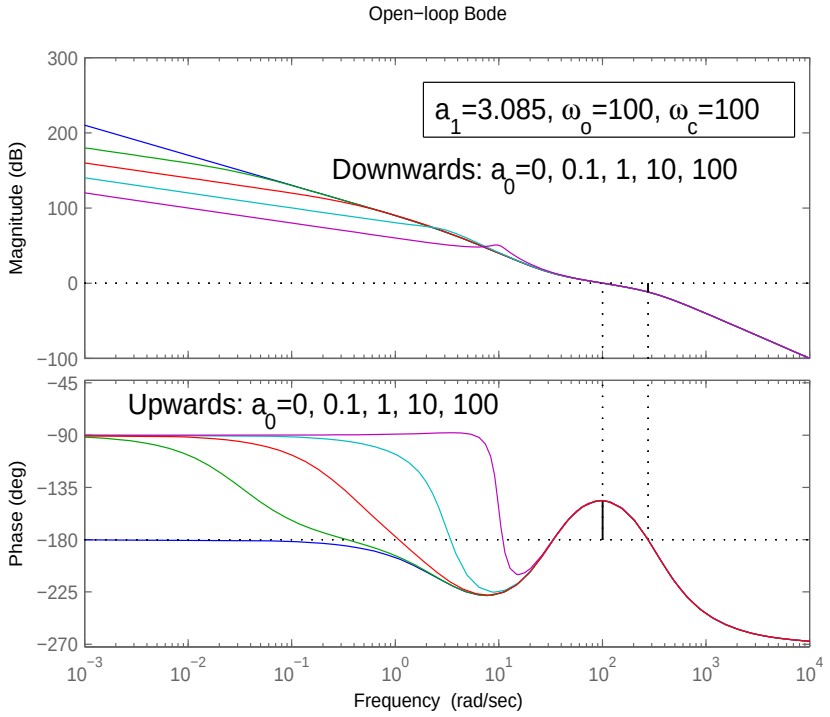

Figure 20: Loop Gain Bode Plots for $a_0 = [0, 0.1, 1, 10, 100]$ (3^{rd}-order ESO)

21, with $\omega_c = \omega_o = 100$ rad/sec, $b = 206.25$, $a_0 = 0$, and $a_1 = [0.1, 1, 3.085, 10, 100]$. The stability margins for each curve in Figure 21 are shown in Table V. Figure 21 and Table V show that gain margin, phase margin and cross-over frequency are just as insensitive to changes in a_1 as to those in a_0.

Table V: Gain Margin and Phase margin under different a_1(3^{rd}-order ESO)

	neg GM dB (rad/sec)	pos GM	PM deg(rad/sec)
a1=0.1	-11.6 (36.5)	11.6 (273)	31.9 (100)
a1=1	-12.0 (35.7)	11.6 (274)	32.5 (100)
a1=3.085	-13.0 (33.6)	11.7 (276)	33.7 (100)
a1=10	-16.9 (26.2)	12.1 (282)	37.6 (99.6)
a1=100	N/A	16.2 (352)	81.2 (53.2)

Now we let a_0 and a_1 change simultaneously, as shown in Figure 22. Again, similar to Figure 20 and Figure 21, the gain margin, phase margin, and cross-over frequency change very little for different combinations of a_0 and a_1.

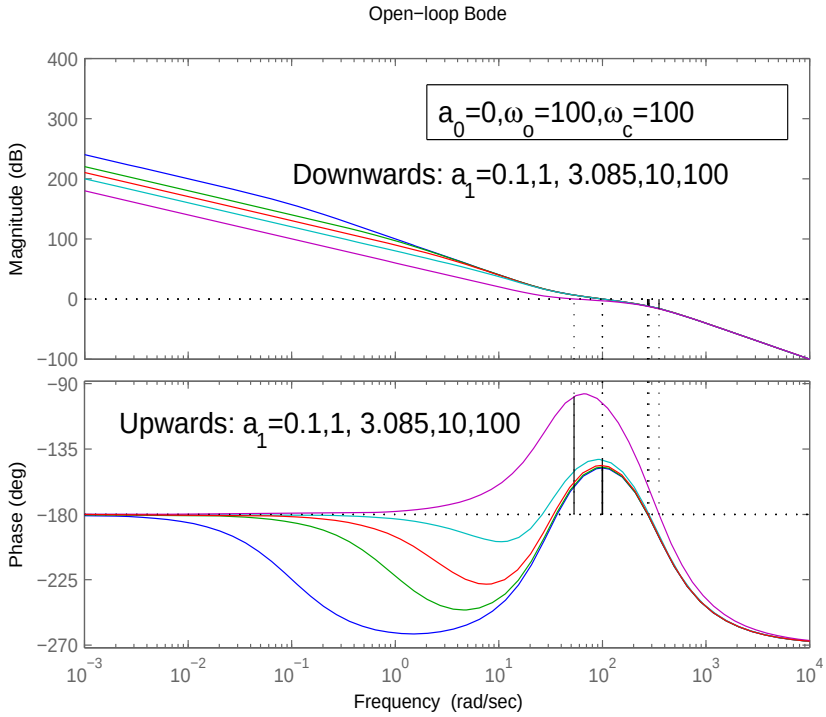

Figure 21: Loop Gain Bode Plots for $a_1 = [0.1, 1, 3.085, 10, 100]$ (3^{rd}-order ESO)

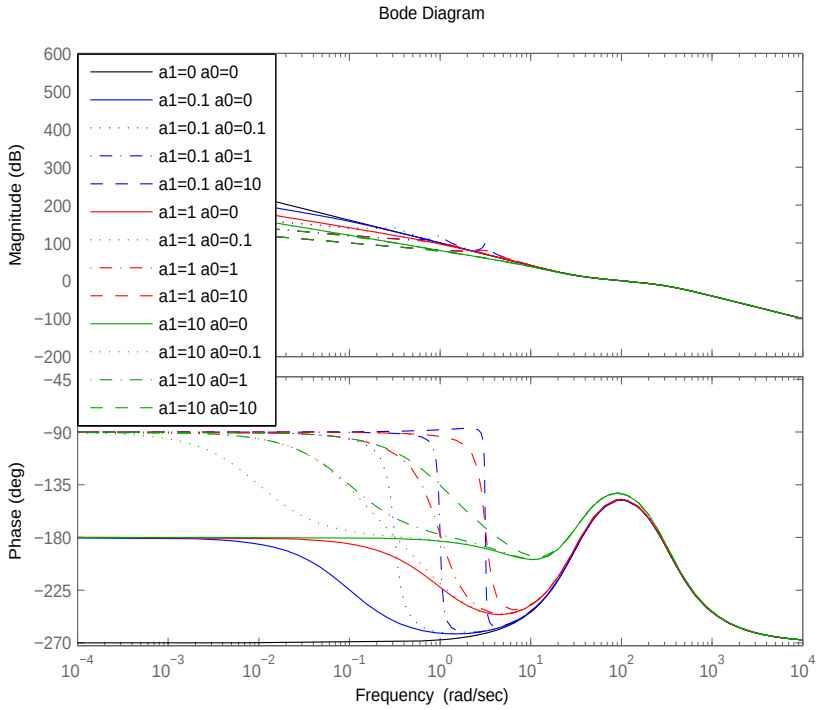

Figure 22: Loop Gain Bode plots for different a_1 and a_0(3^{rd}-order ESO)

Finally, as to the ratio $\rho = b/\hat{b}$, since $\hat{b}$ is fixed, it is proportional to the uncertainties in the plant parameter b. The open-loop transfer function (4.5) shows that the influence of ρ on it is a constant gain factor. Thus the gain margins indicate that the upper and lower limits for the acceptable variations in ρ.

4.1.3 External Disturbance Rejection

In this section we show that consistent input disturbance rejection is achieved even in the presence of significant uncertainties of a_0 and a_1.

The Bode plots of $G_{dy}(s)$ in ADRC (3^{rd}-order ESO) with a_0 and a_1 changing are shown in Figure 23 and Figure 24, respectively, demonstrating excellent disturbance rejection properties that are unaffected by the plant parametric uncertainties.

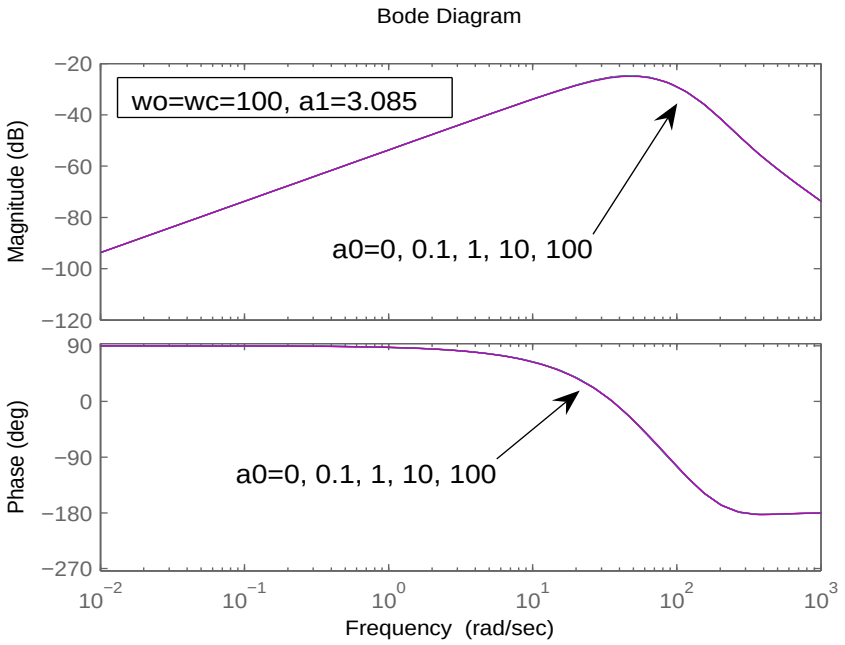

Figure 23: Bode plots of $G_{dy}(s)$ for $a_0 = [0, 0.1, 1, 10, 100]$ (3^{rd}-order ESO)

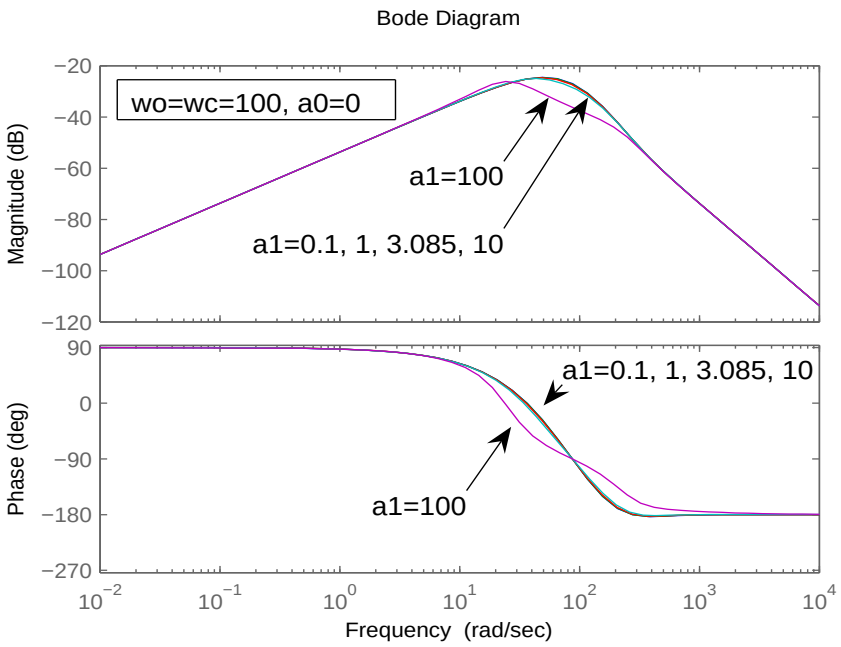

Figure 24: Bode plots of $G_{dy}(s)$ for $a_1 = [0.1, 1, 3.085, 10, 100]$($3^{rd}$-order ESO)

4.2 ADRC with RESO

In this section two ADRC with RESO controllers are investigated: the ADRC with second-order ESO, as described in (3.3), and the ADRC with first-order ESO, as described in (3.5). The 2-dof transfer functions of these two controllers, denoted by $G_{c2}(s)$ and $H_2(s)$, $G_{c1}(s)$ and $H_1(s)$, are obtained from the equations (A.38) and (A.39) respectively, as shown in the following equations.

$$\begin{aligned} G_{c2}(s) &= \frac{1}{\hat{b}} \frac{(\omega_c^2 + 4\omega_c\omega_o + \omega_o^2)s^2 + (2\omega_c^2\omega_o + 2\omega_c\omega_o^2)s + \omega_c^2\omega_o^2}{s(s + 2\omega_o + 2\omega_c)} \\ H_2(s) &= \frac{(s^2 + 2\omega_o s + \omega_o^2)(s^2 + 2\omega_c s + \omega_c^2)}{(\omega_c^2 + 4\omega_c\omega_o + \omega_o^2)s^2 + (2\omega_c^2\omega_o + 2\omega_c\omega_o^2)s + \omega_c^2\omega_o^2} \end{aligned} \tag{4.8}$$

$$\begin{aligned} G_{c1}(s) &= \frac{1}{\hat{b}} \frac{(2\omega_c + \omega_o)s^2 + (\omega_c^2 + 2\omega_c\omega_o)s + \omega_c^2\omega_o}{s} \\ H_1(s) &= \frac{(s + \omega_o)(s^2 + 2\omega_c s + \omega_c^2)}{(2\omega_c + \omega_o)s^2 + (\omega_c^2 + 2\omega_c\omega_o)s + \omega_c^2\omega_o} \end{aligned} \tag{4.9}$$

For the first analysis task, the stability boundary search program in *Section 4.1* is used here again for these two ADRC controllers. The results are shown in Figure

25 and Figure 26 respectively.

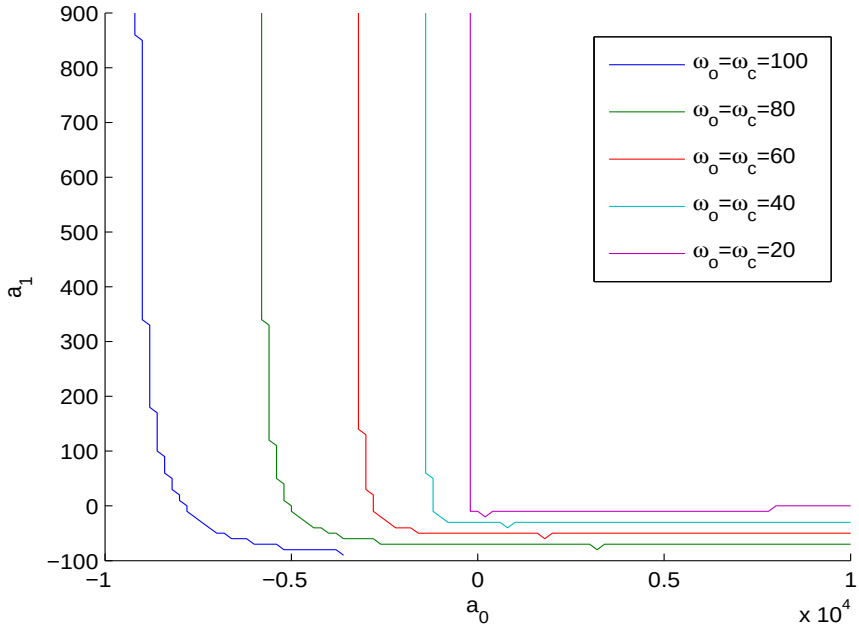

Figure 25: Stability of ADRC(2^{nd}-order RESO) in a_0-a_1 plane

Compare Figure 19, Figure 25, and Figure 26. It shows that, when m decreases, ADRC can tolerate more parametric uncertainties.

Second, the loop gain study in *Section 4.1.2* is repeated for the two ADRC controllers, as shown in Figure 27 and Figure 28, Figure 29 and Figure 30, respectively.

The loop gain plots show that, the ADRC with RESO controllers have the same insensitivity of gain margin, phase margin, and cross-over frequency towards a_0 and a_1 as the ADRC with ESO controller. However,the two ADRC with RESO controllers present a different characteristics from the ADRC with ESO controller: the phase curves do not cross $-180°$ when gain margin is positive, which means the upper bound of ρ does not exist.

Finally, the task in *Section 4.1.3* is carried out for ADRC controllers with 2^{nd}-order and 1^{st}-order ESO. Together with the curves in Figure 23 and Figure 24, Bode

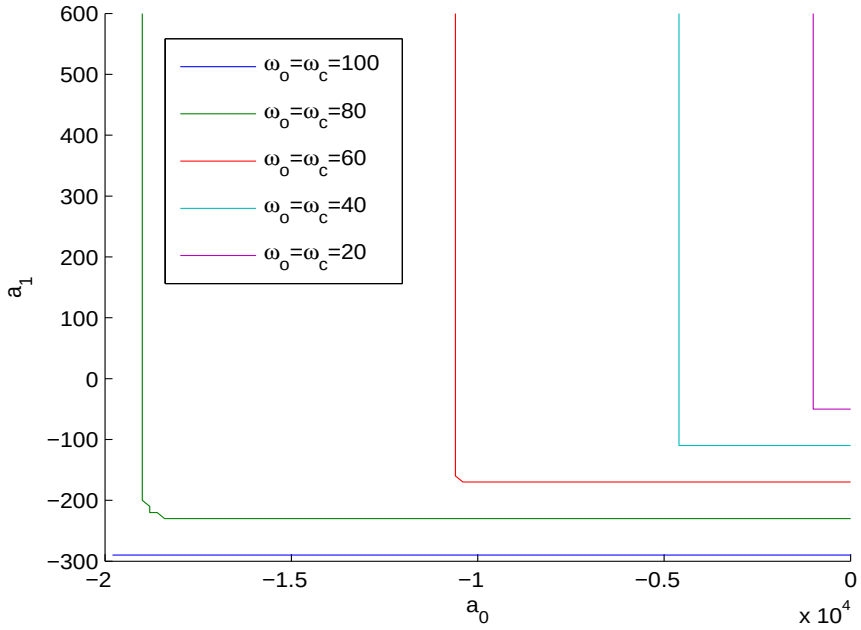

Figure 26: Stability of ADRC(1^{st}-order RESO) in a_0-a_1 plane

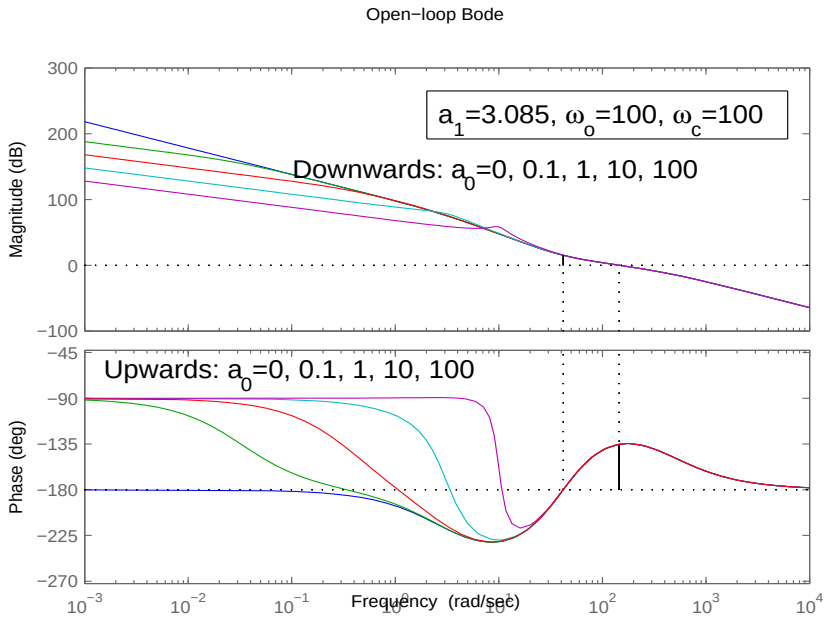

Figure 27: Loop Gain Bode Plots for $a_0 = [0, 0.1, 1, 10, 100]$ (2^{nd}-order ESO)

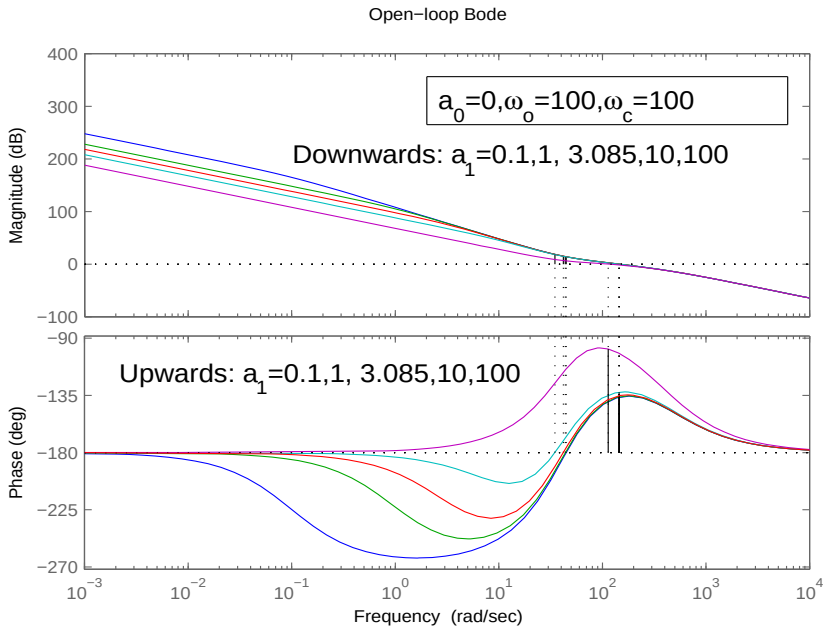

Figure 28: Loop Gain Bode Plots for $a_1 = [0.1, 1, 3.085, 10, 100]$ (2^{nd}-order ESO)

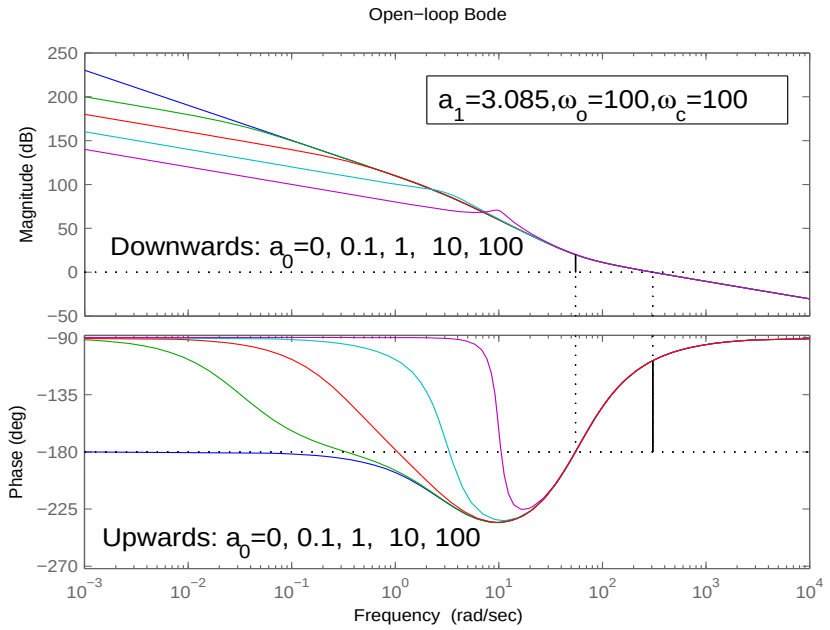

Figure 29: Loop Gain Bode Plots for $a_0 = [0, 0.1, 1, 10, 100]$ (1^{st}-order ESO)

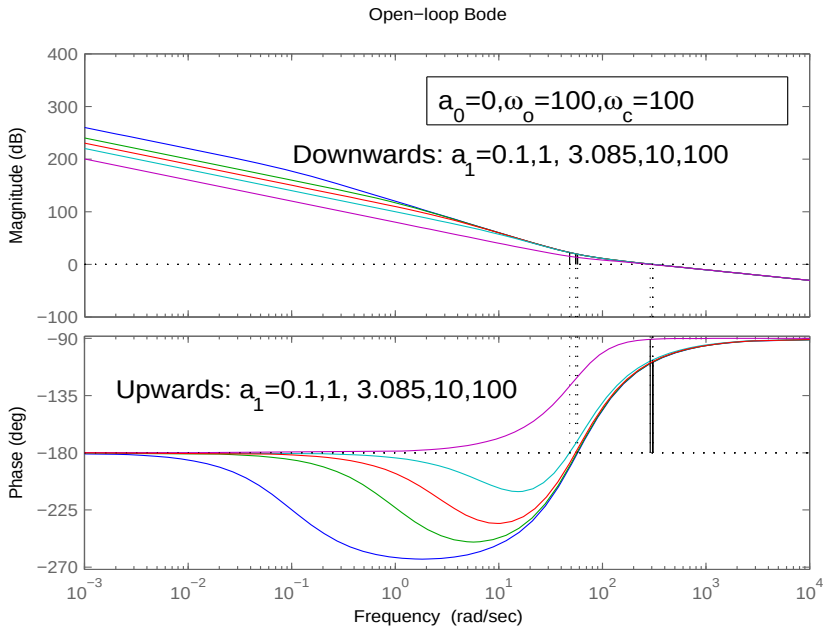

Figure 30: Loop Gain Bode Plots for $a_1 = [0.1, 1, 3.085, 10, 100]$ (1^{st}-order ESO)

plots of $G_{dy}(s)$ are plotted in the following figure.

The input disturbance sensitivity transfer functions plots in Figure 31 shows that, when the order of the ESO decreases, the external disturbance rejection ability of ADRC improves.

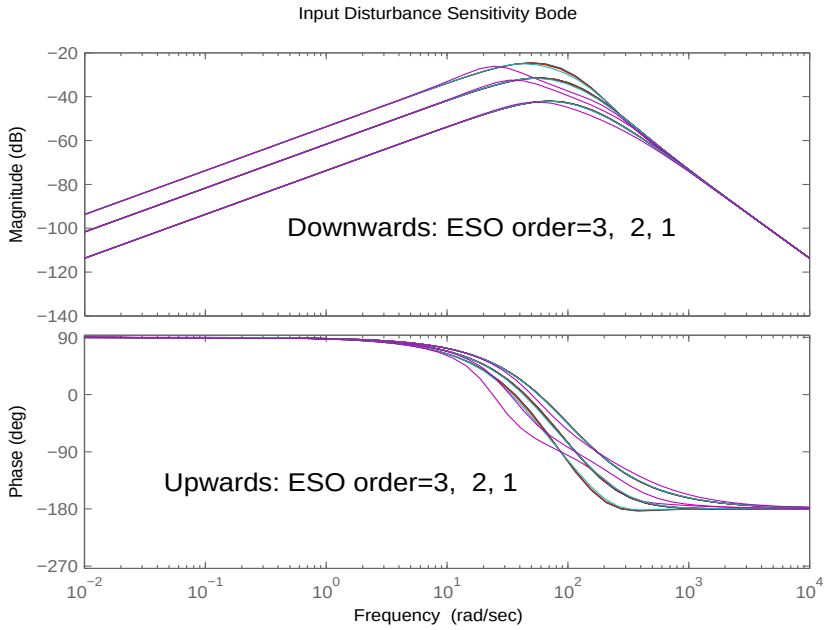

Figure 31: Bode plots of $G_{dy}(s)$ for ADRC (3^{rd}-order, 2^{nd}-order, and 1^{st}-order ESO)

CHAPTER V

SUMMARY AND FUTURE RESEARCH

5.1 Conclusions

The disturbance estimation and rejection problem is the focus of this thesis. An extensive review of various existing disturbance estimation methods is conducted. The advantages and disadvantages of each method are discussed. Comparisons among these methods show that, all previous methods assume LTI environment except ADRC, which presents obvious advantages over the other methods. Besides its ability of dealing with nonlinearities and its state-feedback-control manner, ADRC also provides a very simple and easy way to implement itself. This benefit comes from the two-parameter tuning and no requirement for nominal plant model.

In order to decrease phase lag in the ESO, reduced-order observer technique is applied, defined as RESO. To make it easy to do frequency response analysis for ADRC controller with RESO, general transfer functions are derived for n^{th}-order plant. This enables ADRC, a method developed and analyzed only in time domain in the past due to the nonlinearities, to be analyzed in frequency domain. The transfer

functions show that when the order of the ESO is reduced, the phase lag in it decreases as desired. With the transfer functions, mapping between DoB Q filter design and ESO design in disturbance rejection aspect under LTI environment are also available. The trasfer function study also shows that ME is covered by the general ADRC-RESO structure. With these conditional equivalence between ADRC and the other methods, the stability proof of ADRC can benefit these methods.

The derived 2dof transfer functions allow the ADRC controllers to be evaluated, against a 2^{nd}-order SISO LTI plant with parametric uncertainties, using the classical transfer function and frequency response techniques. Explaining and examining a new control concept in a language practicing engineers are familiar with proves to be effective. It is shown that the stability robustness in the presence of parametric uncertainties clearly improves as the controller and observer bandwidth increases. More importantly, the loop gain frequency response shows a remarkable level of consistency in bandwidth and stability margins against significant parameter variations in the plant. Similar consistency is also found in the disturbance rejection performance.

Although ADRC is generally applicable to nonlinear, time-varying, n^{th}-order systems with multiple-input and multiple-output, applying it to a SISO LTI plant demonstrates how powerful the new idea is. Many modern control techniques reduce to an equivalent classical loop-shaping design with no improvement, when they are applied to a SISO LTI plant. ADRC proves otherwise. It even produces a much better solution in SISO design. The promise of estimating and canceling the *generalized disturbance* in the time-domain formulation of ADRC is convincingly confirmed in this frequency response analysis.

5.2 Future Research

Based on the work of this thesis, the following directions are recommended for future investigation. First, similar to the work in [18], the ADRC with proposed RESO can be used for decoupling control in MIMO systems. Second, with the 2dof transfer functions derived in this thesis, the frequency response analysis of ADRC with ESO or RESO can also be performed for MIMO systems. Finally, the nonlinear gains in the original ADRC can be used in ADRC with RESO to improve its performance.

BIBLIOGRAPHY

[1] N. Wiener, *Cybernetics, Second Edition: or the Control and Communication in the Animal and the Machine ,* 1965

[2] K. J. Astrom, T. Hagglund, *PID Controllers: Theory, Design, and Tuning,* International Society for Measurement and Con, 1995.

[3] S. Skogestad, I. Postlethwaite, *Multivariable Feedback Control: Analysis and Design,* Wiley, 1996

[4] C. Brosilow, B. Joseph, *Techniques of Model-Based Control, 1st edition,*Prentice Hall Ptr, 2002

[5] W.S. Levine, *The Control Handbook,* IEEE Press, 1996

[6] J. Han, "A New Type of Controller: NLPID", Control and Decision, Vol.9, No.6, pp.401-407, 1994. (In Chinese)

[7] J. Han, "A class of extended state observers for uncertain systems," *Control and Decision*, vol. 10, no. 1, pp. 85-88, 1995. (In Chinese)

[8] J. Han, "Nonlinear state error feedback control," *Control and Decision*, vol. 10, no. 3, pp. 221-225, 1995. (In Chinese)

[9] J. Han, "Auto-disturbance rejection control and its applications," *Control and Decision*, vol. 13, no. 1, pp. 19-23, 1998. (In Chinese)

[10] J. Han, "Nonlinear design methods for control systems," *Proc. of the 14th IFAC World Congress*, 1999.

[11] Z. Gao, Y. Huang, and J. Han, "An alternative paradigm for control system design," *Proc. of IEEE conference on Decision and Control*, Volume 5, 4-7 Dec. 2001 Page(s):4578 - 4585

[12] Z. Gao "Scaling and Parameterization Based Controller Tuning," *Proc. of the 2003 American Control Conference*, Volume 6, 4-6 June 2003 Page(s):4989 - 4996

[13] Z. Gao, "Active disturbance rejection control: a paradigm shift in feedback control system design," *Proc. of the 2006 American Control Conference*, pp. 2399-2405, 2006.

[14] R. Mikisovic, A. Radke, Z. Gao, "Discrete Implementation and Generalization of the Extended State Observer", *American Control Conference*, 2006, Volume , Issue , 14-16 June 2006

[15] W. Wang, S. Pan, F. Wang, "A Comparison Study of Two Disturbance Rejection Control Strategies for Hydraulic Position Servo Systems," *Industrial Electronics Society, 30th Annual Conference of IEEE*, Vol: 3, pp: 1993-1996, Nov. 2004

[16] A. Radke, "On Disturbance Estimation and Its Applications in Health Monitoring," Doctoral Dissertation, Cleveland State University, 2006

[17] Q. Zheng, L.Q. Gao, Z. Gao, "On Estimation of Plant Dynamics and Disturbance from Input-Output Data in Real Time, " accepted by *2007 IEEE Multiconference on Systems and Control*

[18] Q. Zheng, Z. Chen and Z. Gao, "A Dynamic Decoupling Control Approach and Its Applications to Chemical Processes," accepted, *American Control Conference*, New York, NY, USA, July, 2007

[19] G.F. Franklin, J.D. Powell, and M. Workman, *Digital Control of Dynamic Systems*, 3^rd ed., Menlo Park, CA: Addison Wesley Longman, Inc., 1998, pp. 328-337

[20] C. Johnson, "Accommodation of External Disturbances in Linear Regulator and Servomechanism Problems," *IEEE Trans. Autonm. Control*, 16(6), pp. 635-644, 1971

[21] J.A. Profeta III, V.G. Vogt, M.H. Mickle, "Disturbance Estimation and Compensation in Linear Systems", *Aerospace and Electronic Systems, IEEE Trans.* Vol. 26, Issue: 2 pp: 225-231 1990

[22] Y. Guan, M. Saif, "A Novel Approach to the Design of Unknown Input Observer," *Automatic Control, IEEE Trans*, Vol. 36, Iss. 5, pp: 632-635, May 1991

[23] E. Schrijver, "Disturbance Observers for Rigid Mechanical Systems: Equivalence, Stability, and Design," *Journal of Dynamic Systems, Measurement, and Control, ASME*, Dec. 2002

[24] Umeno, T., and Hori, Y., " Robust Speed Control of DC Servomotors Using Modern Two Degrees-of-Freedom Controller Design," *IEEE Trans. Ind. Election.*, 38, pp. 363-368, , 1991

[25] K. Ohishi et al., "Microprocessor-controlled DC motor for load-insensitive position servo system," *IEEE Trans. Ind. Electron.*, vol.IE-34, pp. 44-49, 1987.

[26] Y. Hori, "Disturbance suppression on acceleration control type DC servosystem," presented at *IEEE PESC88*, session IIB-5, Kyoto, Japan, 1988.

[27] H. Lee, and M. Tomizuka, "Robust Motion Controller Design for High-Accuracy Positioning Systems", *IEEE Trans. Ind. Electron.*, 43, pp. 48-55, 1996

[28] J. Cheong, Y. Youm, W.K. Chung, "Joint Tracking Controller for Multi-Link Flexible Robot Using Disturbance Observer and Parameter Adaptation Scheme," *Journal of Robotic Systems*, Vol. 19, Issue 8 , pp: 401-417, 2002

[29] K. Yang, Y. Choi, W.K. Chung, I.H. Suh, S.R. Oh, "On the Tracking Performance Improvement of Optical Disk Drive Servo Systems Using Error-Based Disturbance Observer," *Industrial Electronics, IEEE Tran.*, Vol. 52, Issue. 1, pp: 270- 279, FEBRUARY 2005.

[30] S. Kwon, W. K. Chung and Y. Youm, "A novel robust tracking controller based on hierarchical perturbation compensation", *American Control Conference, Proceedings of the 2001*, Vol. 1, pp. 541-546

[31] S. Kwon, W.K. Chung "A Discrete-Time Design and Analysis of Perturbation Observer for Motion Control Applications," *Control Systems Technology, IEEE Tran.*, Vol. 11, No. 3, pp. 399-407, 2003

[32] S. Kwon, "Robust Kalman filtering with perturbation estimation process for uncertain systems," *Control Theory and Applications, IEE Proceedings- Publication*, 2006, Vol. 153, Issue: 5, pp. 600-606

[33] A. Tornambe, P. Valigi, "A Decentralized Controller for the Robust Stabilization of a Class of MIMO Dynamical Systems," *ASME, Journal of Dynamic Systems, Measurement, and Control*. Vol. 116, no. 2, pp. 293-304. June 1994

[34] R. Bickel, and M. Tomizuka, "Passivity-Based Versus Disturbance Observer Based Robot Control: Equivalence and Stability," *ASME, Journal of Dynamic Systems, Measurement*, and Control, 121, pp. 41-47. 1999

[35] Q. Zheng, L.Q. Gao, Z. Gao, "On stability analysis of Active Disturbance Rejection Control for nonlinear time-varying plants with unknown dynamics, " submitted for publication.

[36] D.G. Luenberger, "An Introduction to Observers," *Automatic Control, IEEE Trans.*, Vol. AC-16,pp. 596-602, 1971

APPENDIX

APPENDIX A

TRANSFER FUNCTION DERIVATION

Continue with the equation (3.20).

ESO has two inputs. The first one is u_1. the second input is the estimation of $x_{n+h-m+1}$, which is $y^{(n)} + n^{(n)} - u_1$ when ESO order equals to the extended state number ($m = h$), or $y^{(n+h-m)} + n^{(n+h-m)}$ when ESO order is greater than the extended state number ($m > h$).

Here the two different conditions are treated respectively in the following two sections. However, the derivation result of these two different conditions is consistent and can be merged later.

Define w as the row number of vectors or matrices, which is used in the equation derivation. Also define $\Psi_{x,y}^{m} = \sum_{i=x}^{y} l_i s^{m-i}$ to make derivation easier, where $0 \leq x \leq y$.

A.1 Relative order of ESO Equals to one

In this case, $m = h$, $x_{n+h-m+1} = x_{n+1} = y^{(n)} + n^{(n)} - u_1$ and (3.14) is written as follows.

$$\begin{cases} \dot{z} = A_z z + B_z u_1 + L\left(y^{(n)} + n^{(n)} - u_1 - C_z z\right) \\ \hat{f} = Vz \end{cases} \tag{A.1}$$

A.1.1 ESO estimation after disturbance cancellation

substitute $U(s) = (U_0(s) - VZ(s))/\hat{b}$ and $U_1(s) = U_0(s) - VZ(s)$ into the Laplace transform of (3.17) and (A.1) respective to get the follows.

$$(s^2 - F(s))Y(s) = \rho\left(U_0(s) - VZ(s)\right) + bD(s) \tag{A.2}$$

$$sZ(s) = A_z Z(s) - LU_0(s) + Ls^{(n)}\left(Y(s) + N(s)\right) \tag{A.3}$$

Rearrange (A.3) and substitute Define $M = (sI - A_z)^{-1}$ to get the following equation.

$$Z(s) = -MLU_0(s) + MLs^{(n)}\left(Y(s) + N(s)\right) \tag{A.4}$$

Substitute (A.4) into (A.2) and get

$$Y(s) = \frac{\rho\left(1 + VML\right)U_0(s) + bD(s) - \rho VMLs^n N(s)}{s^n - F(s) + \rho VMLs^n} \tag{A.5}$$

The matrices needed in (A.4) and (A.5) calculation are derived as following.

$$M = \begin{bmatrix} s & -1 & 0 & \cdots & 0 \\ 0 & s & -1 & \cdots & 0 \\ 0 & 0 & s & \ddots & \vdots \\ \vdots & \vdots & \ddots & \ddots & -1 \\ 0 & 0 & 0 & \cdots & s \end{bmatrix}^{-1} = \frac{1}{s^m} \begin{bmatrix} s^{m-1} & s^{m-2} & s^{m-3} & \cdots & 1 \\ 0 & s^{m-1} & s^{m-2} & \cdots & s \\ 0 & 0 & s^{m-1} & \ddots & s^2 \\ \vdots & \vdots & \ddots & \ddots & \vdots \\ 0 & 0 & 0 & \cdots & s^{m-1} \end{bmatrix}$$

$$ML = \frac{1}{s^m}\begin{bmatrix} s^{m-1} & s^{m-2} & s^{m-3} & \cdots & 1 \\ 0 & s^{m-1} & s^{m-2} & \cdots & s \\ 0 & 0 & s^{m-1} & \ddots & s^2 \\ \vdots & \vdots & \ddots & \ddots & \vdots \\ 0 & 0 & 0 & \cdots & s^{m-1} \end{bmatrix}\begin{bmatrix} l_1 \\ l_2 \\ \vdots \\ l_m \end{bmatrix} = \frac{1}{\Psi^m_{0,0}}\begin{bmatrix} \Psi^m_{1,m} \\ \vdots \\ s^{w-1}\Psi^m_{w,m} \\ \vdots \\ s^{m-1}\Psi^m_{m,m} \end{bmatrix}$$

where w denotes the row number.

$$VML = \begin{bmatrix} 1 & 0 & \cdots & 0 \end{bmatrix}\frac{1}{\Psi^m_{0,0}}\begin{bmatrix} \Psi^m_{1,m} \\ \vdots \\ s^{w-1}\Psi^m_{w,m} \\ \vdots \\ s^{m-1}\Psi^m_{m,m} \end{bmatrix} = \frac{\Psi^m_{1,m}}{\Psi^m_{0,0}}$$

$$1 + VML = 1 + \frac{\Psi^m_{1,m}}{\Psi^m_{0,0}} = \frac{\Psi^m_{0,m}}{\Psi^m_{0,0}}$$

Substitute the above matrices into (A.5) and get the follows.

$$Y(s) = \frac{\rho\left(U_0(s) + \hat{b}\frac{\Psi^m_{0,0}}{\Psi^m_{0,m}}D_i(s) - \frac{\Psi^m_{1,m}}{\Psi^m_{0,m}}s^n N(s)\right)}{s^n + (\rho-1)s^n\frac{\Psi^m_{1,m}}{\Psi^m_{0,m}} + F(s)\frac{\Psi^m_{0,0}}{\Psi^m_{0,m}}} \tag{A.6}$$

The transfer functions in Figure 17 are then obtained as follows.

$$G_{p0}(s) = \frac{\rho}{s^n + (\rho-1)s^n\frac{\Psi^m_{1,m}}{\Psi^m_{0,m}} + F(s)\frac{\Psi^m_{0,0}}{\Psi^m_{0,m}}} \tag{A.7}$$

$$G_d(s) = \hat{b}\frac{\Psi^m_{0,0}}{\Psi^m_{0,m}} \tag{A.8}$$

$$G_n(s) = -\frac{\Psi^m_{1,m}}{\Psi^m_{0,m}}s^n \tag{A.9}$$

Substitute (A.6) into (A.4) and (3.20). Then the observer state vector and the

augmented plant state vector can be expressed by $U_0(s)$, $D(s)$ and $N(s)$.

$$Z(s) = \frac{\frac{1}{\Psi^m_{0,m}} \begin{bmatrix} \Psi^m_{1,m} \\ \vdots \\ s^{w-1}\Psi^m_{w,m} \\ \vdots \\ s^{m-1}\Psi^m_{m,m} \end{bmatrix} \left(\left((\rho-1)s^n + F(s)\right)U_0(s) + s^n b D(s) + s^n(s^n - F(s))N(s)\right)}{s^n - \frac{\Psi^m_{0,0}}{\Psi^m_{0,m}}F(s) + (\rho-1)\frac{\Psi^m_{1,m}}{\Psi^m_{0,m}}s^n} \tag{A.10}$$

$$X = \frac{\begin{bmatrix} \rho \\ \vdots \\ \rho s^{w-1} \\ \vdots \\ \rho s^{n-1} \\ s^{(n+1)-1}(\rho - 1 + s^{-n}F(s)) \\ \vdots \\ s^{w-1}(\rho - 1 + s^{-n}F(s)) \\ \vdots \\ s^{(n+h)-1}(\rho - 1 + s^{-n}F(s)) \end{bmatrix} \left(U_0(s) - \frac{\Psi^m_{1,m}}{\Psi^m_{0,m}}s^n N(s)\right) + \begin{bmatrix} 1 \\ \vdots \\ s^{w-1} \\ \vdots \\ s^{n-1} \\ s^{(n+1)-1}\frac{\Psi^m_{0,m}}{\Psi^m_{0,0}} \\ \vdots \\ s^{w-1}\frac{\Psi^m_{0,m}}{\Psi^m_{0,0}} \\ \vdots \\ s^{(n+h)-1}\frac{\Psi^m_{0,m}}{\Psi^m_{0,0}} \end{bmatrix} \frac{\Psi^m_{0,0}}{\Psi^m_{0,m}} b D(s)}{s^n + (\rho-1)s^n\frac{\Psi^m_{m-h+1,m}}{\Psi^m_{0,m}} - F(s)\frac{\Psi^m_{0,m-h}}{\Psi^m_{0,m}}} \tag{A.11}$$

A.1.2 2-dof transfer function derivation

Substitute $m = h$ into the Laplace transform of (3.15) to get the follows.

$$U_0(s) = \sum_{i=1}^{n+1} k_i s^{i-1} R(s) - \sum_{i=1}^{n} k_i s^{i-1} Y(s) \tag{A.12}$$

According to Figure 17, the relationship between r, y, and u_0 is as follows.

$$U_0(s) = H_0(s)G_{c0}(s)R(s) - G_{c0}Y(s) \tag{A.13}$$

Compare (A.12) and (A.13). The 2-dof transfer functions with respect to $U_0(s)$ are obtained as follows.

$$G_{c0}(s) = \sum_{i=1}^{n} k_i s^{i-1} \tag{A.14}$$

$$H_0(s) = \frac{\sum_{i=1}^{n+1} k_i s^{i-1}}{\sum_{i=1}^{n} k_i s^{i-1}} \tag{A.15}$$

Now Derive $G_c(s)$ and $H(s)$ based on $G_{c0}(s)$ and $H_0(s)$ as shown in Figure 16.

$$\begin{aligned}
\hat{b}U(s) &= U_1(s) = U_0(s) - Z_1(s) = \frac{\Psi_{0,m}^m}{\Psi_{0,0}^m}U_0(s) - \frac{s^n\Psi_{1,m}^m}{\Psi_{0,0}^m}Y(s) \\
&= \frac{\Psi_{0,m}^m}{\Psi_{0,0}^m}\sum_{i=1}^{n+1} k_i s^{i-1}R(s) - \frac{\Psi_{0,m}^m}{\Psi_{0,0}^m}\sum_{i=1}^{n} k_i s^{i-1}Y(s) - \frac{s^n\Psi_{1,m}^m}{\Psi_{0,0}^m}Y(s) \\
&= \frac{\Psi_{0,m}^m \sum_{i=1}^{n+1} k_i s^{i-1}}{\Psi_{0,0}^m}R(s) - \frac{\Psi_{0,m}^m \sum_{i=1}^{n} k_i s^{i-1}Y(s) + s^n\Psi_{1,m}^m}{\Psi_{0,0}^m}Y(s)
\end{aligned}$$

$$U(s) = \frac{1}{\hat{b}}\frac{\Psi_{0,m}^m \sum_{i=1}^{n+1} k_i s^{i-1}}{\Psi_{0,0}^m}R(s) - \frac{1}{\hat{b}}\frac{\Psi_{0,m}^m \sum_{i=1}^{n} k_i s^{i-1}Y(s) + s^n\Psi_{1,m}^m}{\Psi_{0,0}^m}Y(s) \tag{A.16}$$

In Figure 18, the control signal $U(s)$ is generated from $R(s)$ and $Y(s)$ as follows.

$$U(s) = H(s)G_c(s)R(s) - G_c(s)Y(s) \tag{A.17}$$

Compare (A.17) and (A.16) and get the 2-dof transfer functions with respect to U.

$$G_c(s) = \frac{1}{\hat{b}}\frac{\Psi_{0,m}^m \sum_{i=1}^{n} k_i s^{i-1}Y(s) + s^n\Psi_{1,m}^m}{\Psi_{0,0}^m} \tag{A.18}$$

$$H(s) = \frac{\Psi_{0,m}^m \sum_{i=1}^{n+1} k_i s^{i-1}}{\Psi_{0,m}^m \sum_{i=1}^{n} k_i s^{i-1}Y(s) + s^n\Psi_{1,m}^m} \tag{A.19}$$

A.2 Relative Order of ESO is Greater Than One

In this case, $m > h$, $x_{n+h-m+1} = y^{(n+h-m)} + n^{(n+h-m)}$ and (3.14) is written as follows.

$$\begin{cases} \dot{z} = A_z z + B_z u_1 + L\left(y^{(n+h-m)} + n^{(n+h-m)} - C_z z\right) \\ \hat{f} = Vz \end{cases} \tag{A.20}$$

Define $K_r = \sum_{i=1}^{n+1} k_i s^{(i-1)}$, $K_y = \sum_{i=1}^{n+h-m} k_i s^{(i-1)}$,

$$K_z = \begin{bmatrix} k_{n+h-m+1} & \cdots & k_n & 0 & \cdots & 0 \end{bmatrix}_{1\times m}$$

There is an exception: when $m = n + h$ all the feedback signals calculated in u are from ESO outputs. Thus define $K_y = \sum_{i=1}^{n+h-m} k_i s^{(i-1)} = 0$ when $m = n + h$.

The Laplace transform of (3.15) is then written as follows.

$$U_0(s) = K_r R(s) - K_y Y(s) - K_z Z(s) \tag{A.21}$$

A.2.1 ESO estimation after disturbance cancellation

substitute $U(s) = (U_0(s) - VZ(s))/\hat{b}$ into the Laplace transform of (3.17) and get the same result as (A.2).

Substitute $U_1(s) = U_0(s) - VZ(s)$ in observer state space equations (A.20)and get $sZ(s) = AZ(s) + B_0\left(U_0(s) - VZ(s)\right) + L\left(s^{(n+h-m)}(Y(s) + N(s)) - CZ(s)\right)$.

Rearrange the above equation and substitute $M = (sI - A_z + LC_z + B_z V)^{-1}$ into it to get the following equation.

$$Z(s) = MB_z U_0(s) + MLs^{(n+h-m)}\left(Y(s) + N(s)\right) \tag{A.22}$$

Substitute (A.22) into (A.2) and rearrange the above equation to get the follows.

$$Y(s) = \frac{\left(1 - VMB_z\right)\rho U_0(s) + bD(s) - \rho VMLs^{(n+h-m)}N(s)}{s^n - F(s) + \rho VMLs^{(n+h-m)}} \tag{A.23}$$

The matrices needed in (A.22) and (A.23) calculation are derived as following.

$$M = (sI - A_z + LC_z + B_zV)^{-1} = \begin{bmatrix} s+l_1 & -1 & 0 & \cdots & 0 \\ l_2 & s & 0_{m-h,m-h+1} & \cdots & 0 \\ l_3 & 0 & s & \ddots & \vdots \\ \vdots & \vdots & \ddots & \ddots & -1 \\ l_m & 0 & 0 & \cdots & s \end{bmatrix}^{-1}_{m\times m}$$

$$= \frac{1}{\Psi^m_{0,m-h}} \begin{bmatrix} M_{11} & 0 \\ M_{21} & M_{22} \end{bmatrix}_{m\times m}$$

where

$$M_{11} = \begin{bmatrix} s^{-1}\Psi^m_{0,0} & s^{-2}\Psi^m_{0,0} & \cdots & s^{-(m-h)}\Psi^m_{0,0} \\ -\Psi^m_{2,m-h} & s^{-1}\Psi^m_{0,1} & \cdots & s^{-(m-h-1)}\Psi^m_{0,1} \\ \vdots & \vdots & \ddots & \vdots \\ -s^{m-h-2}\Psi^m_{m-h,m-h} & -s^{m-h-3}\Psi^m_{m-h,m-h} & \cdots & s^{-1}\Psi^m_{0,m-h-1} \end{bmatrix}_{(m-h)\times(m-h)}$$

$$M_{21} = \begin{bmatrix} -s^{m-h-1}\Psi^m_{m-h+1,m} & -s^{m-h-2}\Psi^m_{m-h+1,m} & \cdots & -\Psi^m_{m-h+1,m} \\ \vdots & \vdots & \ddots & \vdots \\ -s^{m-3}\Psi^m_{m-1,m} & -s^{m-4}\Psi^m_{m-1,m} & \cdots & -s^{h-2}\Psi^m_{m-1,m} \\ -s^{m-2}\Psi^m_{m,m} & -s^{m-3}\Psi^m_{m,m} & \cdots & -s^{h-1}\Psi^m_{m,m} \end{bmatrix}_{h\times(m-h)}$$

$$M_{22} = \begin{bmatrix} s^{-1}\Psi^m_{0,m-h} & s^{-2}\Psi^m_{0,m-h} & \cdots & s^{-h}\Psi^m_{0,m-h} \\ 0 & s^{-1}\Psi^m_{0,m-h} & \ddots & \vdots \\ \vdots & \ddots & \ddots & s^{-2}\Psi^m_{0,m-h} \\ 0 & \cdots & 0 & s^{-1}\Psi^m_{0,m-h} \end{bmatrix}_{h\times h}$$

$$VM = \frac{1}{\Psi^m_{0,m-h}} \begin{bmatrix} -s^{m-h-1}\Psi^m_{m-h+1,m} & \cdots & -\Psi^m_{m-h+1,m} & s^{-1}\Psi^m_{0,m-h} & \cdots & s^{-h}\Psi^m_{0,m-h} \end{bmatrix}_{1\times m}$$

$$MB_z = \frac{1}{\Psi^m_{0,m-h}} \begin{bmatrix} s^{-(m-h)}\Psi^m_{0,0} \\ \vdots \\ s^{-(m-h+1-w)}\Psi^m_{0,w-1} \\ \vdots \\ s^{-1}\Psi^m_{0,m-h-1} \\ -s^{0}\Psi^m_{m-h+1,m} \\ \vdots \\ -s^{h-1+w-m}\Psi^m_{w,m} \\ \vdots \\ -s^{h-1}\Psi^m_{m,m} \end{bmatrix}_{m\times 1}$$

$$1 - VMB_z = 1 - \frac{-\Psi^m_{m-h+1,m}}{\Psi^m_{0,m-h}} = \frac{\Psi^m_{0,m-h}+\Psi^m_{m-h+1,m}}{\Psi^m_{0,m-h}} = \frac{\Psi^m_{0,m}}{\Psi^m_{0,m-h}}$$

Split L into two vectors. $L = \begin{bmatrix} L_1 \\ L_2 \end{bmatrix}$ where L_1 is $(m-h)\times 1$ and L_2 is $(h)\times 1$.

$$ML s^{(n+h-m)} = \frac{s^{(n+h-m)}}{\Psi^m_{0,m-h}} \begin{bmatrix} M_{11} & 0 \\ M_{21} & M_{22} \end{bmatrix} \begin{bmatrix} L_1 \\ L_2 \end{bmatrix} = \frac{s^{(n+h-m)}}{\Psi^m_{0,m-h}} \begin{bmatrix} M_{11}L_1 \\ M_{21}L_1 + M_{22}L_2 \end{bmatrix}$$

$$= \frac{s^{(n+h-m)}}{\Psi^m_{0,m-h}} \begin{bmatrix} \sum_{i=1}^{m-h} l_i s^{m-i} \\ \vdots \\ \sum_{i=w}^{m-h} l_i s^{w-1-i}\Psi^m_{0,w-1} - \sum_{i=1}^{w-1} l_i s^{w-1-i}\Psi^m_{w,m-h} \\ \vdots \\ \sum_{i=m-h}^{m-h} l_i s^{m-h-1-i}\Psi^m_{0,m-h-1} - \sum_{i=1}^{m-h-1} l_i s^{m-h-1-i}\Psi^m_{m-h,m-h} \\ \sum_{i=m-h+1}^{m} l_i s^{m-h-i}\Psi^m_{0,m-h} - \sum_{i=1}^{m-h} l_i s^{m-h-i}\Psi^m_{m-h+1,m} \\ \vdots \\ \sum_{i=w}^{m} l_i s^{w-1-i}\Psi^m_{0,m-h} - \sum_{i=1}^{m-h} l_i s^{w-1-i}\Psi^m_{w,m} \\ \vdots \\ \sum_{i=m}^{m} l_i s^{m-1-i}\Psi^m_{0,m-h} - \sum_{i=1}^{m-h} l_i s^{m-1-i}\Psi^m_{m,m} \end{bmatrix}_{m\times 1}$$

$$= \frac{s^{(n+h-m)}}{\Psi^m_{0,m-h}} \begin{bmatrix} \Psi^m_{1,m-h} \\ \vdots \\ s^{w-1-m}\Psi^m_{w,m-h}\Psi^m_{0,w-1} - s^{w-1-m}\Psi^m_{1,w-1}\Psi^m_{w,m-h} \\ \vdots \\ s^{-h-1}\Psi^m_{m-h,m-h}\Psi^m_{0,m-h-1} - s^{-h-1}\Psi^m_{1,m-h-1}\Psi^m_{m-h,m-h} \\ s^{-h}\Psi^m_{m-h+1,m}\Psi^m_{0,m-h} - s^{-h}\Psi^m_{1,m-h}\Psi^m_{m-h+1,m} \\ \vdots \\ s^{w-1-m}\Psi^m_{w,m}\Psi^m_{0,m-h} - s^{w-1-m}\Psi^m_{1,m-h}\Psi^m_{w,m} \\ \vdots \\ s^{-1}\Psi^m_{m,m}\Psi^m_{0,m-h} - s^{-1}\Psi^m_{1,m-h}\Psi^m_{m,m} \end{bmatrix}_{m\times 1}$$

$$= \frac{s^{(n+h-m)}}{\Psi^m_{0,m-h}} \begin{bmatrix} \Psi^m_{1,m-h} \\ \vdots \\ s^{w-1-m}\Psi^m_{w,m-h}\Psi^m_{0,0} \\ \vdots \\ s^{-h-1}\Psi^m_{m-h,m-h}\Psi^m_{0,0} \\ s^{-h}\Psi^m_{m-h+1,m}\Psi^m_{0,0} \\ \vdots \\ s^{w-1-m}\Psi^m_{w,m}\Psi^m_{0,0} \\ \vdots \\ s^{-1}\Psi^m_{m,m}\Psi^m_{0,0} \end{bmatrix} = \frac{s^{(n+h-m)}}{\Psi^m_{0,m-h}} \begin{bmatrix} \Psi^m_{1,m-h} \\ \vdots \\ s^{w-1}\Psi^m_{w,m-h} \\ \vdots \\ s^{m-h-1}\Psi^m_{m-h,m-h} \\ s^{m-h}\Psi^m_{m-h+1,m} \\ \vdots \\ s^{w-1}\Psi^m_{w,m} \\ \vdots \\ s^{m-1}\Psi^m_{m,m} \end{bmatrix}_{m\times 1}$$

where q is the row number.

$$VMLs^{n+h-m} = \frac{s^n\Psi^m_{m-h+1,m}}{\Psi^m_{0,m-h}}$$

Substitute the above matrices into (A.23) and get the follows.

$$Y(s) = \frac{\rho U_0(s) + \frac{\Psi^m_{0,m-h}}{\Psi^m_{0,m}} bD(s) - \rho\frac{\Psi^m_{m-h+1,m}}{\Psi^m_{0,m}} s^n N(s)}{s^n + (\rho-1)s^n\frac{\Psi^m_{m-h+1,m}}{\Psi^m_{0,m}} - F(s)\frac{\Psi^m_{0,m-h}}{\Psi^m_{0,m}}} \tag{A.24}$$

The transfer functions in Figure 17 are then obtained as follows.

$$G_{p0}(s) = \frac{\rho}{s^n + (\rho-1)s^n\frac{\Psi^m_{m-h+1,m}}{\Psi^m_{0,m}} - F(s)\frac{\Psi^m_{0,m-h}}{\Psi^m_{0,m}}} \tag{A.25}$$

$$G_d(s) = \hat{b}\frac{\Psi^m_{0,m-h}}{\Psi^m_{0,m}} \tag{A.26}$$

$$G_n(s) = -\frac{\Psi^m_{m-h+1,m}}{\Psi^m_{0,m}} s^n \tag{A.27}$$

Substitute (A.24) into (A.22) and (3.20). Then the observer state vector and

the augmented plant state vector can be expressed by $U_0(s)$, $D(s)$ and $N(s)$.

$$
\begin{aligned}
Z(s) &= MB_0U_0(s) + MLs^{(n+h-m)}\left(Y(s)+N(s)\right) \\
&= \frac{\begin{bmatrix}
s^{n+h-m}\left(1+(\rho-1)\frac{\Psi^m_{1,m}}{\Psi^m_{0,m}}\right) - F(s)\frac{s^{h-m}\Psi^m_{0,0}}{\Psi^m_{0,m}} \\
\vdots \\
s^{n+h-1+w-m}\left(1+(\rho-1)\frac{\Psi^m_{w,m}}{\Psi^m_{0,m}}\right) - F(s)\frac{s^{h-1+w-m}\Psi^m_{0,w-1}}{\Psi^m_{0,m}} \\
\vdots \\
s^{n-1}\left(1+(\rho-1)\frac{\Psi^m_{w,m}}{\Psi^m_{0,m}}\right) - F(s)\frac{s^{-1}\Psi^m_{0,m-h-1}}{\Psi^m_{0,m}} \\
s^{n}(\rho-1)\frac{\Psi^m_{m-h+1,m}}{\Psi^m_{0,m}} + F(s)\frac{\Psi^m_{m-h+1,m}}{\Psi^m_{0,m}} \\
\vdots \\
s^{n+h-1+w-m}(\rho-1)\frac{\Psi^m_{w,m}}{\Psi^m_{0,m}} + F(s)s^{h-1+w-m}\frac{\Psi^m_{w,m}}{\Psi^m_{0,m}} \\
\vdots \\
s^{n+h-1}(\rho-1)\frac{\Psi^m_{m,m}}{\Psi^m_{0,m}} + F(s)s^{h-1}\frac{\Psi^m_{m,m}}{\Psi^m_{0,m}}
\end{bmatrix} U_0(s)}{s^n+(\rho-1)s^n\frac{\Psi^m_{m-h+1,m}}{\Psi^m_{0,m}} - F(s)\frac{\Psi^m_{0,m-h}}{\Psi^m_{0,m}}} \\
&+ \frac{\begin{bmatrix}
s^{n+h-m}\frac{\Psi^m_{1,m-h}}{\Psi^m_{0,m}} \\
\vdots \\
s^{n+h-1+w-m}\frac{\Psi^m_{w,m-h}}{\Psi^m_{0,m}} \\
\vdots \\
s^{n-1}\frac{\Psi^m_{m-h,m-h}}{\Psi^m_{0,m}} \\
s^{n}\frac{\Psi^m_{m-h+1,m}}{\Psi^m_{0,m}} \\
\vdots \\
s^{n+h-1+w-m}\frac{\Psi^m_{w,m}}{\Psi^m_{0,m}} \\
\vdots \\
s^{n+h-1}\frac{\Psi^m_{m,m}}{\Psi^m_{0,m}}
\end{bmatrix} (bD_i(s)+(s^n-F(s))N(s))}{s^n+(\rho-1)s^n\frac{\Psi^m_{m-h+1,m}}{\Psi^m_{0,m}} - F(s)\frac{\Psi^m_{0,m-h}}{\Psi^m_{0,m}}}
\end{aligned}
\tag{A.28}
$$

$$X(s) = \frac{\begin{bmatrix} \rho \\ \vdots \\ \rho s^{w-1} \\ \vdots \\ \rho s^{n-1} \\ s^{(n+1)-1}(\rho-1) + s^{(n+1)-1-n}F(s) \\ \vdots \\ s^{w-1}(\rho-1) + s^{w-1-n}F(s) \\ \vdots \\ s^{(n+h)-1}(\rho-1) + s^{(n+h)-1-n}F(s) \end{bmatrix} U_0(s) + \begin{bmatrix} 1 \\ \vdots \\ s^{w-1} \\ \vdots \\ s^{n-1} \\ s^{(n+1)-1}\frac{\Psi^m_{0,m}}{\Psi^m_{0,m-h}} \\ \vdots \\ s^{w-1}\frac{\Psi^m_{0,m}}{\Psi^m_{0,m-h}} \\ \vdots \\ s^{(n+h)-1}\frac{\Psi^m_{0,m}}{\Psi^m_{0,m-h}} \end{bmatrix} \frac{\Psi^m_{0,m-h}}{\Psi^m_{0,m}} bD_i(s)}{s^n + (\rho-1)s^n \frac{\Psi^m_{m-h+1,m}}{\Psi^m_{0,m}} - F(s)\frac{\Psi^m_{0,m-h}}{\Psi^m_{0,m}}}$$

$$- \frac{\begin{bmatrix} \rho \\ \vdots \\ \rho s^{w-1} \\ \vdots \\ \rho s^{n-1} \\ s^{(n+1)-1}(\rho-1) + s^{(n+1)-1-n}F(s) \\ \vdots \\ s^{w-1}(\rho-1) + s^{w-1-n}F(s) \\ \vdots \\ s^{n+h-1}(\rho-1) + s^{(n+h)-1-n}F(s) \end{bmatrix} \frac{\Psi^m_{m-h+1,m}}{\Psi^m_{0,m}} s^n N(s)}{s^n + (\rho-1)s^n \frac{\Psi^m_{m-h+1,m}}{\Psi^m_{0,m}} - F(s)\frac{\Psi^m_{0,m-h}}{\Psi^m_{0,m}}} \tag{A.29}$$

A.2.2 2-dof transfer function derivation

Substitute (A.22) into (A.21) and get the follows.

$$U_0(s) = \frac{K_r R(s) - \left(K_y + K_z M L s^{n+h-m}\right) Y(s)}{1 + K_z M B_z} \tag{A.30}$$

The items needed in (A.30) are derived as follows.

$$1 + K_z M B_z = 1 + \begin{bmatrix} k_{n+h-m+1} & \cdots & k_n & 0 & \cdots & 0 \end{bmatrix} \frac{1}{\Psi^m_{0,m-h}} \begin{bmatrix} s^{-(m-h)}\Psi^m_{0,0} \\ \vdots \\ s^{-(m-h+1-w)}\Psi^m_{0,w-1} \\ \vdots \\ s^{-1}\Psi^m_{0,m-h-1} \\ -s^{0}\Psi^m_{m-h+1,m} \\ \vdots \\ -s^{h-1+w-m}\Psi^m_{w,m} \\ \vdots \\ -s^{h-1}\Psi^m_{m,m} \end{bmatrix}$$

$$= 1 + \frac{\sum_{j=1}^{m-h} k_{n+h-m+j} s^{-(m-h+1-j)} \Psi^m_{0,j-1}}{\Psi^m_{0,m-h}} = \frac{\Psi^m_{0,m-h} + \sum_{j=1}^{m-h} k_{n+h-m+j} s^{h-1+j-m} \Psi^m_{0,j-1}}{\Psi^m_{0,m-h}}$$

$$= \frac{\sum_{j=1}^{m-h+1} k_{n+h-m+j} s^{h-1+j-m} \Psi^m_{0,j-1}}{\Psi^m_{0,m-h}}$$

$$K_y + K_z M L s^{(n+1-m)}$$

$$= \sum_{i=1}^{n+h-m} k_i s^{(i-1)} + \begin{bmatrix} k_{n+h-m+1} & \cdots & k_n & 0 & \cdots & 0 \end{bmatrix} \frac{s^{(n+h-m)}}{\Psi^m_{0,m-h}} \begin{bmatrix} \Psi^m_{1,m-h} \\ \vdots \\ s^{w-1}\Psi^m_{w,m-h} \\ \vdots \\ s^{m-h-1}\Psi^m_{m-h,m-h} \\ s^{m-h}\Psi^m_{m-h+1,m} \\ \vdots \\ s^{w-1}\Psi^m_{w,m} \\ \vdots \\ s^{m-1}\Psi^m_{m,m} \end{bmatrix}$$

$$= \frac{\sum_{j=1}^{n+h-m} k_j s^{(j-1)} \Psi^m_{0,m-h} + s^{(n+h-m)} \sum_{j=1}^{m-h} k_{n+h-m+j} s^{j-1} \Psi^m_{j,m-h}}{\Psi^m_{0,m-h}}$$

Substitute $1 + K_z M B_z$, $K_y + K_z M L s^{(n+1-m)}$, and K_r into (A.30) and get the follows.

$$U_0(s) = \frac{\Psi^m_{0,m-h} \sum_{j=1}^{n+1} k_j s^{(j-1)}}{\sum_{j=1}^{m-h+1} k_{n+h-m+j} s^{j-m} \Psi^m_{0,j-1}} R(s) - \frac{\sum_{j=1}^{n+h-m} k_j s^{(j-1)} \Psi^m_{0,m-h} + s^{(n+h-m)} \sum_{j=1}^{m-h} k_{n+h-m+j} s^{j-1} \Psi^m_{j,m-h}}{\sum_{j=1}^{m-h+1} k_{n+h-m+j} s^{j-m} \Psi^m_{0,j-1}} Y(s) \tag{A.31}$$

Compare (A.32) and (A.13) and get the 2-dof transfer functions with respect

to u_0 as follows.

$$G_{c0}(s) = \frac{\sum_{j=1}^{n+h-m} k_j s^{j-1}\Psi^m_{0,m-h} + s^{n+h-m}\sum_{j=1}^{m-h} k_{n+h-m+j}s^{j-1}\Psi^m_{j,m-h}}{\sum_{j=1}^{m-h+1} k_{n+h-m+j}s^{h-1+j-m}\Psi^m_{0,j-1}} \quad (A.32)$$

$$H_0(s) = \frac{\Psi^m_{0,m-h}\sum_{j=1}^{n+1} k_j s^{j-1}}{\sum_{j=1}^{n+h-m} k_j s^{j-1}\Psi^m_{0,m-h} + s^{n+h-m}\sum_{j=1}^{m-h} k_{n+h-m+j}s^{j-1}\Psi^m_{j,m-h}} \quad (A.33)$$

Substitute MB_z and ML into (A.22) and get the follows.

$$Z_m(s) = \frac{-\Psi^m_{m-h+1,m}}{\Psi^m_{0,m-h}}U_0(s) + \frac{s^n\Psi^m_{m-h+1,m}}{\Psi^m_{0,m-h}}Y(s)$$

$$\hat{b}U(s) = U_1(s) = U_0(s) - Z_m(s) = \frac{\Psi^m_{0,m}}{\Psi^m_{0,m-h}}U_0(s) - \frac{s^n\Psi^m_{m-h+1,m}}{\Psi^m_{0,m-h}}Y(s) \quad (A.34)$$

Substitute (A.32) into (A.34)and get the following equation.

$$U(s) = \frac{1}{\hat{b}}\frac{\Psi^m_{0,m}}{\Psi^m_{0,m-h}}H_0C_0R(s) - \frac{1}{\hat{b}}\left(\frac{\Psi^m_{0,m}}{\Psi^m_{0,m-h}}C_0(s) + \frac{\Psi^m_{0,m}}{\Psi^m_{0,m-h}}s^n\right)Y(s) \quad (A.35)$$

$$= \frac{1}{\hat{b}}\frac{\Psi^m_{0,m}\sum_{j=1}^{n+1} k_j s^{(j-1)}}{\sum_{j=1}^{m-h+1} k_{n+h-m+j}s^{j-m}\Psi^m_{0,j-1}}R(s)$$

$$-\frac{1}{\hat{b}}\frac{\Psi^m_{0,m}\sum_{j=1}^{n+h-m} k_j s^{(j-1)} + \sum_{j=1}^{m-h+1} k_{n+h-m+j}s^{n+h-1-m+j}\Psi^m_{j,m}}{\sum_{j=1}^{m-h+1} k_{n+h-m+j}s^{j-m}\Psi^m_{0,j-1}}Y(s)$$

Compare (A.36) and (A.17) and get the 2-dof transfer functions with respect to u as follows.

$$G_c(s) = \frac{1}{\hat{b}}\frac{\Psi^m_{0,m}\sum_{j=1}^{n+h-m} k_j s^{(j-1)} + \sum_{j=1}^{m-h+1} k_{n+h-m+j}s^{n+h-1-m+j}\Psi^m_{j,m}}{\sum_{j=1}^{m-h+1} k_{n+h-m+j}s^{h-1+j-m}\Psi^m_{0,j-1}} \quad (A.36)$$

$$H(s) = \frac{\Psi^m_{0,m}\sum_{j=1}^{n+1} k_j s^{(j-1)}}{\Psi^m_{0,m}\sum_{j=1}^{n+h-m} k_j s^{(j-1)} + \sum_{j=1}^{m-h+1} k_{n+h-m+j}s^{n+h-1-m+j}\Psi^m_{j,m}} \quad (A.37)$$

where $1 \leq h$, $h < m \leq n+h$, and $\sum_{i=1}^{n+h-m} k_i s^{(i-1)} = 0$ when $m = n+h$.

A.3 Merge

Comparing (A.6) with (A.24), (A.10) with (A.28), (A.11) with (A.29), (A.18)with (A.36) and (A.19)with (A.37), it's easy to see that the case that $m = h$ can be merged into the case $m > h$. The only modification is to change the condition to $1 \leq h \leq m$.

Thus the 2-dof equivalent transfer function of ADRC are the follows.

$$G_c(s) = \frac{1}{\hat{b}} \frac{\Psi_{0,m}^m \sum_{j=1}^{n+h-m} k_j s^{(j-1)} + \sum_{j=1}^{m-h+1} k_{n+h-m+j} s^{n+h-1-m+j} \Psi_{j,m}^m}{\sum_{j=1}^{m-h+1} k_{n+h-m+j} s^{h-1+j-m} \Psi_{0,j-1}^m} \quad \text{(A.38)}$$

$$H(s) = \frac{\Psi_{0,m}^m \sum_{j=1}^{n+1} k_j s^{(j-1)}}{\Psi_{0,m}^m \sum_{j=1}^{n+h-m} k_j s^{(j-1)} + \sum_{j=1}^{m-h+1} k_{n+h-m+j} s^{n+h-1-m+j} \Psi_{j,m}^m} \quad \text{(A.39)}$$

where $1 \leq h$, $h \leq m \leq n+h$, and $\sum_{i=1}^{n+h-m} k_i s^{(i-1)} = 0$ when $m = n+h$.